IEEE Access
Multidisciplinary | Rapid Review | Open Access Journal

Date of publication xxxx 00, 0000, date of current version xxxx 00, 0000.

Digital Object Identifier 10.1109/ACCESS.2017.Doi Number

High-Voltage Pulse Generators for Electroporation Applications: A Systematic Review

M.R. Qasemian Reyhan Abadi[1], M. Hoseintabar Marzebali[1], V. Abolghasemi[2], Senior Member, IEEE, M. H. Anisi[2], Senior Member, IEEE

[1]Facualty of Electrical Engineering, Shahrood University of Technology, Shahrood, IRAN
[2]School of Computer Science and Electronic Engineering (CSEE), University of ESSEX, Colchester, UK

Corresponding author: M. Hoseintabar Marzebali (m.hoseintabar@shahroodut.ac.ir)

ABSTRACT In recent years, the use of electroporation process has attracted much attention, due to its application in various industrial and medical fields. Electroporation is a microbiology technique which creates tiny holes in the cell membrane by the applied electric field. The electroporation process needs high-voltage pulses to provide the required electric field. To generate high-voltage pulses, a pulse generator device must be used. High-voltage pulse generators can be mainly divided into two major groups: Classical pulse generators and power electronics-based pulse generators. As their name suggests, the first group is associated with the primary and elementary pulse generators like Marx generators, and the second group is associated with the pulse generators that have been updated with the advancement of power electronics like Modular Multilevel Converters. These two major groups are also divided into several subgroups which are reviewed in detail in this paper. This study reviews the literature presented in the field of pulse power and pulse generators proper for the electroporation process and addresses their strengths and weaknesses. Several tables are provided to highlight and discuss the characteristics of each subgroup. Finally, a comparative study among different groups of pulse generators is performed which is followed by a classification performance analysis.

INDEX TERMS Electroporation, irreversible electroporation, Marx generator, modular multilevel converter, power electronics, pulsed electric field

I. INTRODUCTION

In 1754, by observing the effect of electric sparks on human and animal skin by J.A. Nollet, the phenomenon of electroporation was discovered and described [1]. Electroporation is a proceeding which creates holes in the cell membrane using intense and short electric field pulses, which can have different effects according to the parameters of the applied electric field [2]. The Pulsed Electric Field (PEF) causes tiny pores in the cell membrane [3]. If the applied electric field E is so strong that it is greater than the critical electric field ($E_{critical}$) and the relation $E > E_{critical}$ [4] or $E_{thermal} > E > E_{ire}$ [5] (E_{ire} is the electric field that is necessary to start the electroporation process and $E_{thermal}$ is the electric field that leads to the thermal effects) holds, this leads to cell death, a process called Irreversible Electroporation (IRE), as shown in Fig. 1. Conversely, if the applied electric field does not reach the IRE threshold value, the cell will be able to recover the pores created and return to its previous state, in which case this process is called Reversible Electroporation (RE), as illustrated in Fig. 1. The IRE method is commonly used to kill cells, while the RE method is used to create pores in the tissue and facilitate the exchange process [1]. If electrical field strength E_{ire} satisfies the range of 2.5 KV/cm for mammalian cells, 12 KV/cm for plant cells, and 24 KV/cm for bacteria, then the IRE process will be achieved. Also, for the treatment of IRE in mammalian cells, the pulse width should be in the range of $1\mu s$ to several hundreds of μs and the number of pulses is changeable from 1 to 100 [5].

In general, the applications of electroporation can be divided into two categories [6]: industrial [3], [7]-[17] and medical [3], [18]-[20] applications.

In recent years, various applications have been introduced, developed, or commercialized with the help of pulsed power technology. Fusion systems, food pasteurization (sterilization), water treatment, ozone generation, biofouling prevention, air pollution control, wastewater processing, etc., can be considered as industrial applications of pulsed power [3], [7]-[17]. The biomedical applications of pulsed power are cancer treatment, wound healing, gene transfection, etc. [3], [18]-[20]. Electroporation, gene gun, and microinjection are physical methods of intracellular gene transfer *in vitro* and *in vivo*. Low gene delivery and limitation of the transfected cells to the needle injection site are disadvantages of the needle injection method. High efficiency of transduction, precision of delivery dosage and timing are the advantages of this method. Gene gun is a fast and efficient method of transferring exogenous materials into living tissue. The electroporation method works on a wide range of cell types. This method is safe and does not use biochemical agents but it leads to intensive cell damage and induces immunogenic reactions [21].

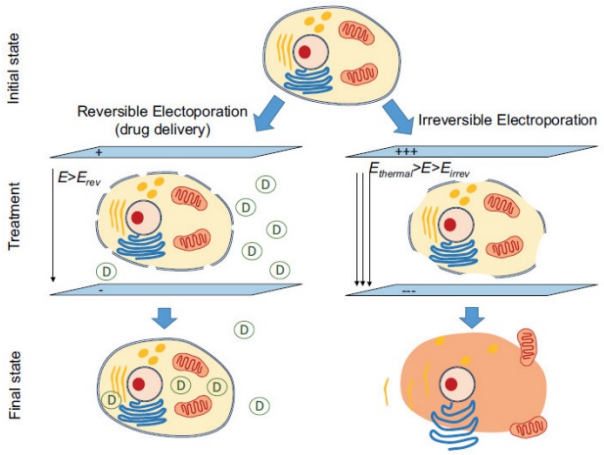

FIGURE 1. Electroporation process: reversible (left) and irreversible (right) [5].

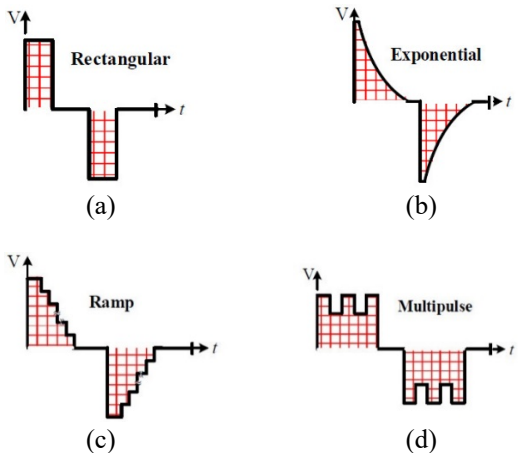

FIGURE 2. Common pulse waveforms in electroporation. (a) Rectangular. (b) Exponential. (c) Ramp. (d) Multipulse [3].

To generate such an electric field, a device called a Pulse Generator (PG) must be used [4]. The electroporation process requires High-Voltage (HV) generators to provide the electric field to generate RE and IRE [22].

In order to cover most applications, a PG should be controllable and flexible, as particular HV pulse requirements are needed depending on the type of application [23]. There is a wide range of HV pulse waveforms that can be used in electroporation. Rectangular, exponential, multi-pulse (combined narrow and wide pulse duration), and ramp pulses are prevalent waveforms as shown in Fig. 2. Among these, the rectangular pulse waveform, shown in Fig. 2(a), is the most prevalent waveform because of its effective pulse area compared to the exponential pulse waveform [3]. Due to the nature of classical PGs, which consist of an RC network, they generate an exponential voltage waveform across the load, as shown in Fig. 2(b). In novel PGs, the specifications of exponential voltage waveforms such as plateau, rise and tail times can be mimicked by ramp waveforms [3], [23], according to Fig. 2(c), therefore they can be used in insulation testing of power system components [23]. By combining wide pulses with a train of narrow pulses, a multipulse waveform is created, as shown in Fig. 2(d), which is used in food sterilization applications, because the amount of heat produced is minimized without altering the food nutrition value [3], [23].

The HV pulses applied in electroporation treatment can be either unipolar or bipolar. In addition to electrical stresses, bipolar pulses cause reversing mechanical stresses in the under-treatment microorganisms, that precipitates the electroporation proceeding [3].

In some publications, PGs are classified based on their operation methodology [24]. With the advent of novel PGs due to progresses in power electronics devices and converters, an updated classification of PGs has been made based on their topological variations [23]. PGs can be divided into two main groups called Classical PGs and power electronics-based PGs. The operation principle of the classical PGs is as follows. Energy is stored in capacitors or inductors, then, this energy is abruptly discharged into the load [24]. Due to the steady development of HV semiconductor switches such as silicon and silicon carbide with high voltage rating and higher switching frequency ability, HV pulses can be generated with the help of power electronics-based converters [3].

Our major contribution in this review is collecting, structuring and discussing a wide range of pulsed power generators classification techniques presented in recent years. In each structure, several different articles have been reviewed to create a better understanding of the different topologies of each group, as well as comparison tables in terms of the number of elements used, the voltage gain and the output waveforms for each structure are collected to give a better view to researchers and readers. In the following subsections, each of the known PGs are described.

II. CLASSICAL HIGH-VOLTAGE PULSE GENERATORS

In essense, charging a group of capacitors in parallel and then discharging the capacitors in series leads to generation of the required HV pulse in classical PGs. Marx generators, Pulse Forming Networks (PFNs), and Blumlein Lines are examples of such classical PGs [3].

A. Marx Generator

The basic Marx generator was built by Erwin Marx in 1923. This generator, as shown in Fig. 3, consists of a group of N capacitors C that are charged in parallel through the charging resistor r_c from the input source V_s. Switching operations are performed by spark gaps that have a breakdown voltage slightly higher than V_s. If a cascade breakdown voltage is generated in the spark gaps, the desired HV pulse is generated due to the connection of a series of charged capacitors [25]-[27]. The first spark gap is deliberately activated and applies a voltage of $2V_s$ at both ends of the second spark gap, leading to its conduction. This action keep till all the spark gaps are shorted, and a voltage pulse of the NV_s appears at the load [3]. The main advantage of the Marx generator is that the spark gaps are synchronized automatically. The value of the total capacitance against the load will be C/N; hence the pulse width is obtained via the mathematical relation $t_p = 0.7RC/N$ [6].

The basic Marx generator produces unipolar pulses that, if bipolar pulses are needed, can use another same stack fed from $-V_s$ voltage and place the load differentially between the outputs of the two stacks [24],[28].

Conventional Marx generators cannot be used in portable sources because they are too bulky and heavy. Hence, Compact Marx Generators (CMGs) are used to generate fast-rising, high-power and high-voltage pulses. CMGs can generate various range of voltages with a low rise-time of nanosecond order. The structure of CMGs consists of charging capacitors, metal body, spark gaps, resistors, and connections [29].

B. Pulse Forming Networks

Due to the nature of the RC network, the generated pulse by the Marx generator is exponential. Therefore, if a pulse waveform close to a rectangular is required, PFN can be used. According to Fig. 4, the PFN consists of N cascaded LC section, which is fed through a voltage source V_s. By storing energy in the LC branches, the power supply switch is disconnected, and the HV switch is connected on the load side and delivers the required pulse [30]-[33]. The duration of the generated pulse is also calculated through the mathematical relation $t_p = 2N\sqrt{LC}$ [3].

C. Blumlein Lines

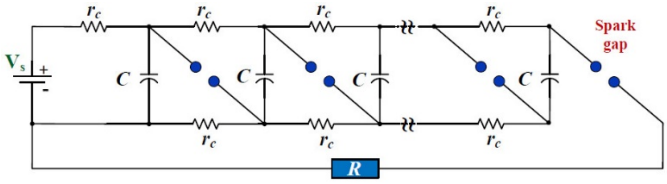

FIGURE 3. Structure of Marx PG [3].

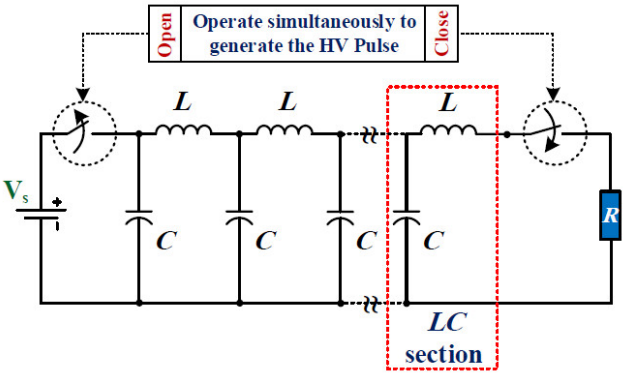

FIGURE 4. Structure of PFN PG [3].

Similar to PFNs, Transmission Lines (TLs) can be used to generate HV pulses [34]-[36]. Requiring load impedance matching to produce near-rectangular pulses, reduces the output pulse voltage peak to half the input voltage. In 1937 Alan Blumlein proposed a solution to make an output pulse voltage peak equal to the input voltage. In this way, the load is placed in series between two identical TLs, and the load impedance must be twice the characteristic impedance of one line ($R = 2Z_0$) [37]-[39].

One of the ways to increase the voltage is to use an induction adder known as Multistage Blumlein Lines (MBLs) [40], [41]. As shown in Fig. 5, this structure uses several pulse transformers whose secondary are series. One of the advantages of this structure is that transformer increases the voltage. Another advantage is that the current is naturally divided between the switches because the transformer cores are independent of each other. This leads to the use of switches with low power ratings. By adding the voltages on the initial side and multiplying it by the transformer turns ratio, the output voltage is obtained [6].

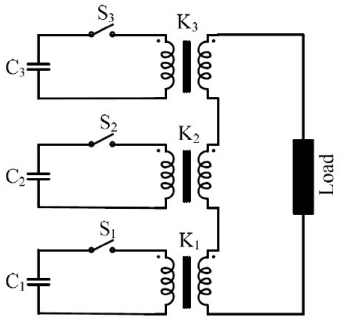

FIGURE 5. Structure of MBL [41].

D. Magnetic Pulse Compressor

The Magnetic Pulse Compressor (MPC) is behaviorally similar to the PFN because both operate on a resonant converter, except that MPC is used to compress the generated pulse with fast rise and fall times. Due to this feature, it can be used in the last stage of the pulse generator unit. In this structure, instead of using gas-state switches, Magnetic Switches (MS) are used. The MPC circuit is shown in Fig. 6 [42]. Assuming the switch is closed under conditions where $C_1 = C_2 = C_3 = C$ and $MS_s << L_1 << MS_u$ (MS_s and MS_u are saturated inductance and unsaturated inductance of magnetic switches, respectively), the energy of the capacitor C_1 that was charged to the voltage V_0 is transferred to the capacitor C_2 under resonance $C-L-C$. Energy transfer from the capacitor C_2 to C_3 occurs when the C_2 potential reaches a point that leads to MS saturation. In the second loop (the right loop in Fig. 6(a)), the switch and L_1 are replaced by the MS. As shown in Fig. 6(b), with the performance of MS during energy transfer, the voltage V_1 (and current I_1) is converted to V_2 (and I_2) and compressed [6].

Magnetic or gas-state switches (non-solid-state) are widely used in pulse power technology, especially in the structures as mentioned earlier, because they have very high electrical strength and fast rise-time. Gas-state switches require vacuum equipment, gas sources, and special operating conditions such as high pressure (≥ 1). These switches are bulky and unreliable, have a short lifespan and low repetition rates. Even though magnetic switches have a higher repetition rate, they still struggle with disadvantages. These disadvantages limit the dynamics and efficiency of structures and lead to increased cost and size of the pulsed power system [10], [43], and [44].

Classical PGs have disadvantages such as low repetition rate, bulkiness, high expense and size, inflexibility, low longevity, and inefficiency [3], [45]. Also, the principal pulse waveform produced in classical PGs is either exponential or rectangular and unipolar [3].

III. HIGH VOLTAGE PULSE GENERATORS BASED ON POWER ELECTRONICS

The commercialization of Gate Turn-Off (GTO) thyristors in the mid-1980s marked the beginning of the development of high-power solid-state converters. GTO was the standard for medium voltage drive before the advent of high-power Insulated-Gate Bipolar Transistors (IGBTs) and Gate-Commutated Thyristors (GCTs) in the late 1990s [46]. The advantages of these switching devices are excellent switching characteristics, ease of gate control, snubberless operation, and reduction of power losses [6].

Solid-state switches have features such as reliability, smaller footprint, high repetition rate, long lifetime, and cost-effectiveness. The use of solid-state switches makes the pulsed power supply smaller and more efficient because it benefits from power electronics controlling techniques [10], [24], [43], [44], and [47].

With the evolvement of power electronics switches in high voltage tolerate and quick on/off switching performance that provides narrow HV pulse generation, several solid-state HV pulse generators have been introduced. Some power electronics-based PGs mimic classical generators, including the Marx generator. Emerging structures and newly developed HV PGs are modular that provide redundancy, scalability, and robust pulse generation operation [3].

Power electronics-based PGs can be divided into three main groups based on the type of structure, namely: Modular Multilevel Converter (MMC) based, Non-MMC-based, and hybrid topologies [3].

A. Non-MMC-Based PG Topologies

Non-MMC-based PGs use power electronic devices to increase the voltage, then a high voltage rated switch connected in series to the load is employed to chop the generated HVDC. Generally, this switch is off, but it is turned on during pulse generation. Hence, the series connection of semiconductor devices is necessary, which is known as the main limitation of this structure [3]. This group of PGs can be divided into three subgroups, namely: Solid-state Marx Pulse Generator (SMPG), Switched-Mode Power Supply (SMPS), and Capacitor-Diode Voltage Multiplier (CDVM) [23]. The conceptual structure of the Non-MMC-based PG is illustrated in Fig. 7.

1. Solid-state Marx Pulse Generator

By imitating the classical Marx generator, studies in solid-state Marx PG have been performed [48]-[53]. The basic idea is that spark gaps in Fig. 3 are replaced by power electronics switches, as shown in Fig. 8 [3].

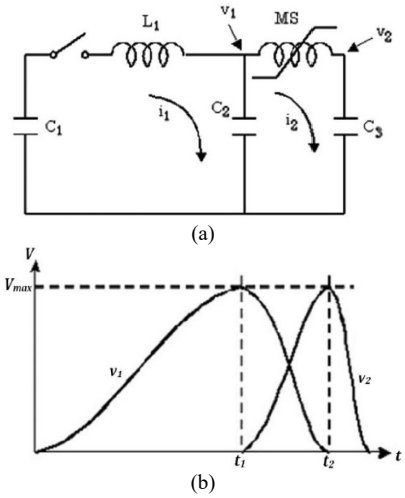

FIGURE 6. Basic structure of MPC. (a) Circuit. (b) Voltage waveforms [42].

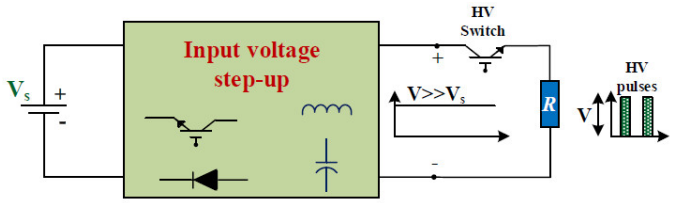

FIGURE 7. Conceptual structure of Non-MMC based PG [3].

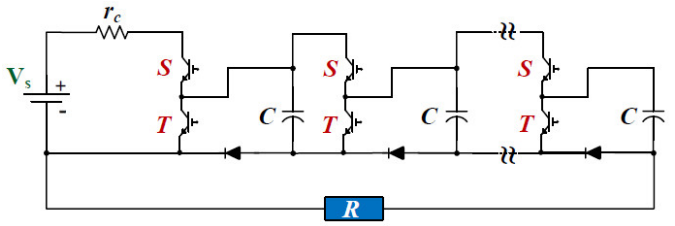

FIGURE 8. Structure of Solid-state Marx PG [3].

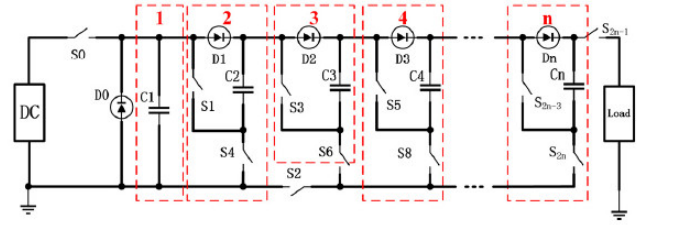

FIGURE 9. Proposed topology in [54] with *n* energy storage capacitors.

The capacitors are charged when switches S are turned on, and the HV pulse is generated when switches T are turned on, as shown in Fig. 8, which provides a controllable charging and discharging mechanism. The main structure of SMPG is such that it generates rectangular unipolar pulses. To generate bipolar pulses in [50] an H-Bridge is used across each capacitor, and in [51], two groups of capacitors are used that are charged from sources with the same voltage level but with reverse polarity.

SMPG has a simple structure [3], and its capacitors are not necessarily fully discharged [23]. This structure suffers from severe voltage drop, which requires control actions or the use of additional passive components [55].

Increasing the output voltage requires more number of capacitors. On the other hand, the weight and size of the all-solid-state Marx generator are mainly determined by capacitors. To achieve a lightweight and compact pulse generator, the number of capacitors needs to be reduced. Therefore, in [54], a modular pulse generator is proposed in which a set of capacitors are charged cyclically, step-by-step, and discharged in series. As shown in Fig. 9, this topology has *n* capacitors, *n* fast recovery diodes, and 2*n*+1 all-solid-state switches that can achieve a voltage gain of 2^{n-1}. That is, the V/C ratio reaches $2^{n-1}/n$. The first unit contains only capacitor C_1. Other units are modules with a capacitor, a fast recovery diode and two all-solid-state switches. The second unit is connected to the third unit in parallel via a solid-state switch. The rest of the units are connected directly in parallel. This structure is a modified Marx circuit. The main difference between this topology and conventional Marx is in the proceeding of charging capacitors because the voltage double charging procedure has been used to increase the voltage of capacitors step-by-step. Charging and discharging stages work independently. The voltage gain is also independent of the input DC source voltage, and the capacitors voltage reaches their maximum before the discharging process begins. As the number of stages increases, the voltage gain increases exponentially, which due to 2^{n-2} charging modes. The number of modes also increases. These lead to the modification of the control strategy and more complexity. This is known as the disadvantage of this topology.

One of the limiting factors of all-solid-state pulse generators application is the rated current of the switches. In order to have a pulse generator with maximum output current, it is necessary to connect several semiconductor switches or pulse generators in parallel to share the current. Current sharing of the paralleled switches is challenging and the surge current due to asynchronous operation may damage the switches. Usually, two groups of switches are adopted to control the discharge of capacitors and form the output pulses, but the topology in [56] is a high-current pulse generator based on Marx generators in parallel that use one group of switches to control the charging of the multiple Marx generators, as shown in Fig. 10. In [56], two schemes are used, namely: scheme (1) and scheme (2). The topology in scheme (1) uses *mn*-stage traditional pulsed Marx generators (which *m* is the number of the Marx generators) in parallel, as shown in Fig. 10(a). Capacitor C_1 of each Marx generator is charged only through diode D_1 and switch S_1, while capacitors C_i are charged via diodes D_1, D_{bi} and D_s, and switches S_1 and S_{bi}. The diode D_s is responsible for cutting off the circulating current between the Marx generators. As shown in Fig. 10(b), in scheme (2), the diodes D_{ai} are replaced by switches S_{bi} in the last stage, and the series S_{bi} switches are placed parallel to the load. The output currents of each Marx generator are different in scheme (1), and the peak output current of scheme (1) is higher than scheme (2). The difference in the output currents of each Marx generator in scheme (2) compared to scheme (1) is relatively small. In order to control the charging proceeding in scheme (2), a set of additional switches have been adopted. System losses in scheme (2) have increased compared to scheme (1). Increasing Marx generators' stages leads to a more balanced output current, which makes the system more stable. In scheme (1), five-sixths of the charging current passes through the measuring branch (branch of cathode side of diode D_s) during the charge cycle. So, the two discharge and charging currents pass through this branch. In scheme (2), all charging currents and discharge currents pass through the measuring branch. S_{bi} switches are responsible for controlling the charge of capacitors and forming output pulses. In the discharge process, the S_{bi} switches are turned off and the S_{ai} switches

are turned on to discharge the capacitors in series to the load. Transistor–Transistor Logic (TTL) signal is used in closed-loop control of the DC power supply to ensure system stability. This structure has the ability to prevent short circuit of the half-bridge circuit to Marx circuit.

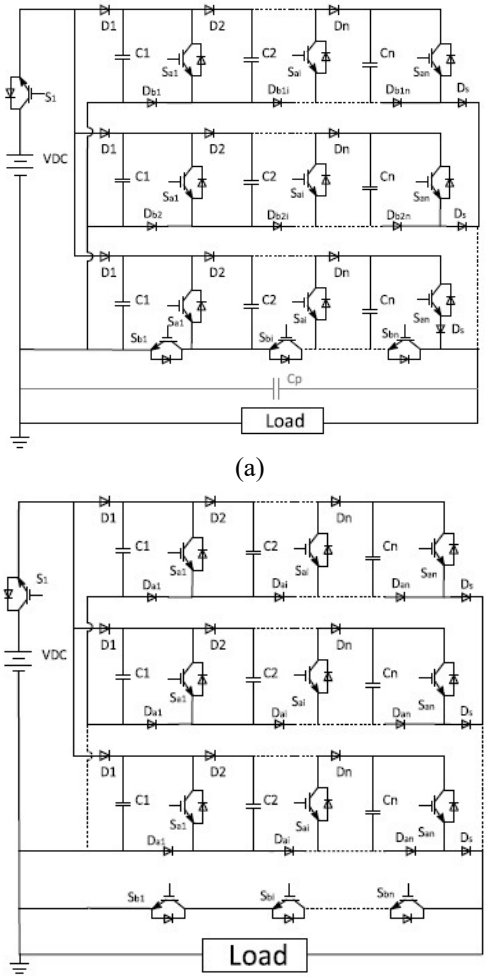

(a)

(b)

FIGURE 10. Structure of *mn*-stage Marx generators in parallel. (a) Scheme (1). (b) Scheme (2) [56].

2. Switched-Mode Power Supply

Studies have been performed on using SMPS to generate HV pulse [57]-[61]. According to Fig. 11, SMPS circuits of the type Boost, Buck-Boost, and Flyback (isolated Buck-Boost) have attracted much attention due to their ability to increase voltage [3].

As shown in Fig. 12(a), in [57], the Boost converter in Discontinuous Conduction Mode (DCM) is used to generate a pulse where the load is placed differentially between the input and output of the converter. This structure generates unipolar pulses and does not require HV switches to generate HV pulses.

According to Fig. 12(b), in [58], the load is located differentially between the outputs of two Boost converters which are so-called front-to-front. This structure has the ability to generate bipolar pulses, but its operation depends on the use of passive elements [47] and requires proper parameter selection [3].

As shown in Fig. 13, in [59] and [60], a Buck-Boost converter is connected to the input source and supplies several Low Voltage (LV) switch–capacitor units at its output side. With proper control of switches Q, it is possible to generate HV pulses with controllable *dv/dt*. This structure generates unipolar pulses and requires a complex control algorithm.

In [61], the Flyback structure shown in Fig. 11(c) has been modified to remove the output filter capacitor and place an *RCD* circuit on the primary side of the transformer, as shown in Fig. 14. The *RCD* circuit, the transformer inductance, and the switch Q form a Buck-Boost converter. When the switch Q is turned on, the primary side of the transformer is connected to the V_s source, and the capacitor of the *RCD* circuit is charged to the following voltage:

$$V_C = \frac{\delta}{1-\delta} V_s \tag{1}$$

where, δ is duty ratio of the switch Q. When the switch Q is turned off, the primary side of the transformer is subjected to the negative voltage of the *RCD* capacitor, and by increasing the voltage due to the transformer turns ratio, it produces a negative unipolar HV pulse across load *R*, which is equal to:

$$V_R = -\frac{n_2}{n_1} \frac{\delta}{1-\delta} V_s \tag{2}$$

where, n_2 and n_1 are secondary and primary turns ratio of the transformer, respectively.

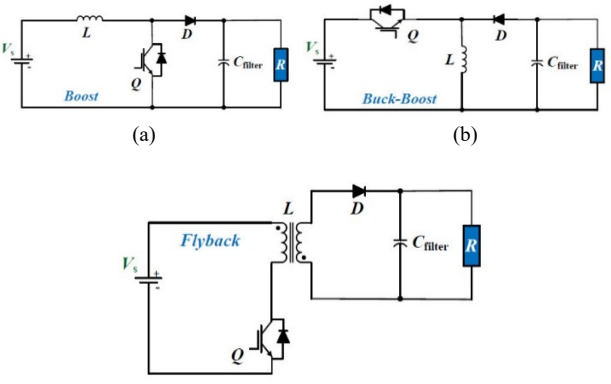

(a) (b)

(c)

FIGURE 11. SMPS circuits for generating HV pulse. (a) Boost. (b) Buck-Boost. (c) Fly-back [3].

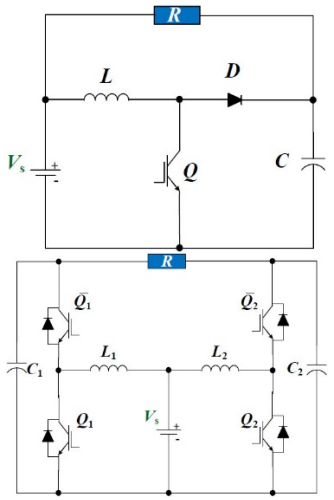

(a) (b)

FIGURE 12. Boost type SMPS circuit. (a) PG based on Boost converter in [57]. (b) PG based on front-to-front Boost converter in [58].

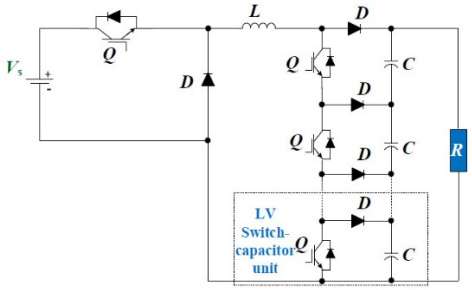

FIGURE 13. PG based on Buck-Boost converter in [59], [60].

3. Capacitor-Diode Voltage Multiplier

The basic CDVM module shown in Fig. 15 is incorporated in the PGs to generate HV pulses [9], [62]-[68]. Typically, CDVM modules use LVDC input to generate HVDC output. An HV switch that is series with load is responsible for chopping the output HVDC [3], which determines the repetition rate and the width of the output pulse [62].

In [62], to achieve higher voltage gain, the Boost converter is used along with the CDVM circuit, which is fed from the AC input of the utility, as shown in Fig. 16. This structure generates unipolar HV pulses using relatively LV elements but requires an HV switch series with load at the output side. Applying closed-loop control in this structure keeps the output voltage constant in different loading conditions and limits the no-load output voltage.

In [63], the Boost converter centrally feeds two groups of CDVM stages symmetrically located on either side of the load terminals. This improves the heat dissipation distribution because it reduces the current change between the CDVM stages.

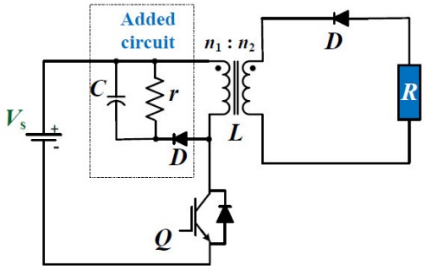

FIGURE 14. PG based on Fly-back [61].

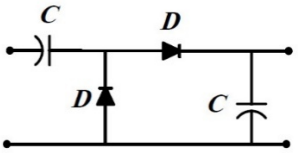

FIGURE 15. Main CDVM module [3].

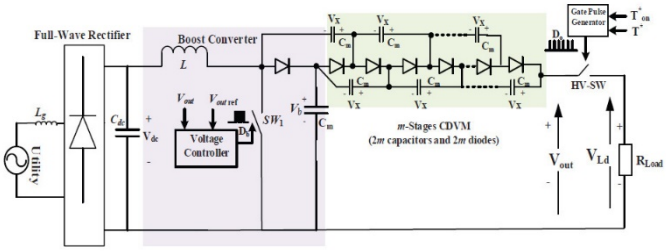

FIGURE 16. CDVM based HV-PG [62].

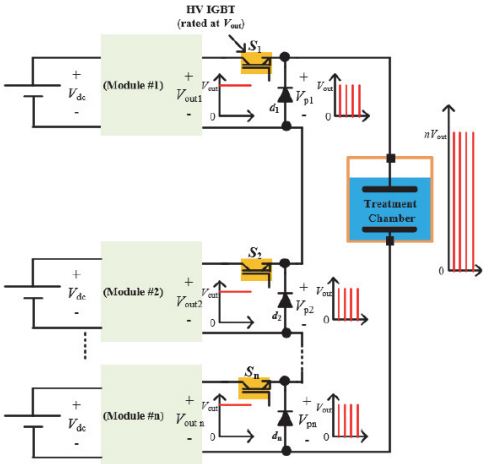

FIGURE 17. PG based on multi-module of CDVM [65].

In [64], the two groups of CDVM stages are symmetrically on either side of the load terminals, one fed by the Boost converter and the other by the Buck-Boost converter. The Buck-Boost converter produces a reverse output relative to the input voltage, which provides series connection of the Boost and Buck-Boost converters outputs without the need for an isolated transformer at the input stage to maximize the output voltage.

Each module of [65], shown in Fig. 17 is the same structure presented in [62]. The output voltage pulses from each module are connected in series and form the total output voltage pulse. This structure has the advantages of

modularity, scalability, and redundancy. For this reason, a diode is placed at the output of each module to prevent any possible interference -between the switches, and in case of failure or deactivation of the modules, it can bypass that module from the circuit.

TABLE I
A COMPARATIVE STUDY BETWEEN CDVM STRUCTURES BASED ON THE NUMBER OF ELEMENTS (n : NUMBER OF BOOST-CDVM MODULES)

Topology	[62]	[63]	[64]	[65]	[9]
No. of stages	m	m	m	m	m
No. of switches	2	2	3	$2n$	$4m$
No. of inductors	1	1	2	n	0
No. of diodes	$2m+1$	$4m+1$	$4m+2$	$2n(m+1)$	$4m$
No. of capacitors	$2m+1$	$4m+1$	$4m+2$	$n(2m+1)$	$2m$

TABLE II
A COMPARATIVE STUDY BETWEEN CDVM STRUCTURES BASED ON VOLTAGE GAIN AND OUTPUT PULSE POLARITY (m : NUMBER OF CDVM STAGES, n : NUMBER OF BOOST-CDVM MODULES AND D_b : BOOST CONVERTER DUTY CYCLE)

Topology	Input voltage	Output voltage	Pulse polarity
[62]	V_{in}	$\left(\frac{m+1}{1-D_b}\right)V_{in}$	Unipolar
[63]	V_{in}	$\left(\frac{2m+1}{1-D_b}\right)V_{in}$	Unipolar
[64]	V_{in}	$\left(\frac{2(m+1)}{1-D_b}-1\right)V_{in}$	Unipolar
[65]	V_{in}	$n\left(\frac{m+1}{1-D_b}\right)V_{in}$	Unipolar
[9]	V_{in}	$(2m-1)V_{in}$	Bipolar

The generated HV pulse in CDVM structures is usually unipolar [62]-[68]. To generate bipolar pulses, the H-bridge can be used in the output stage, where these four switches must be able to withstand the total output pulse voltage level [3], [9].

In [9], a bipolar HV PG, which is a combination of voltage multiplier converter and solid-state LV switches, is presented with a look at the concept of Half-Bridge (HB) inverter as shown in Fig. 18. When the switch T_C^+ is turned on (the other switches are off), the capacitor C_1 is charged through the input source. When the switch T_P^- is turned on, the capacitor C_1 is discharged across the load and generates a positive pulse. When the switch T_C^- is turned on, the capacitor C_2 is charged. When the switch T_P^+ is turned on, the capacitor C_2 is discharged across the load and generates a negative pulse. This structure is modular and flexible.

CDVM structures enjoy advantages such as small size and weight, high efficiency, and reliability [9], [62]-[65]. To perform a comparative study between CDVM structures, Tables I and II have been collected.

According to Table I, the structure of CDVM in [62] has fewer elements, while the structure [65] has more elements. The structure [9] does not require an inductor, which is one of its advantages. As can be seen in Table II, all of the CDVM structures expressed generate unipolar output, while the structure presented in [9] can generate bipolar output. According to Table II, assuming the input voltage source and the number of stages is the same (and $n = m$), the structures [64] and [65] have the highest voltage gain, and the structure [9] have the lowest voltage gain, respectively, while the structures [62], [63] offer the same voltage gain. D_b values are selected based on the table "*Relation between number of stages and duty cycle*" in each paper.

B. MMC-Based PG Topologies

The two-level Voltage Source Converter (VSC) suffers from disadvantages such as bulky input DC capacitor, bulky output ac filter, and high *dv/dt* [3]. Adding additional levels reduces the capacitance of the input capacitor, the size of the harmonic filter, and the *dv/dt* problem [69].

1. MMC Performance Context

MMC is a multilevel VSC structure invented in 2001 by Rainer Marquardt. The MMC structure in terms of hardware is divided into two groups, namely: Half-Bridge Sub-Module (HB-SM) and Full-Bridge Sub-Module (FB-SM) [3]. The structure and switching states of these two types of SM are shown in Fig. 19.

The HB-SM has three switching states, namely: bypass, insertion, and idle, as shown in Fig. 19(a). In the bypass mode, where the switches T_m are on, and switches T_x are off, the SM is short-circuited, and the AB terminal voltage is near zero. In the insertion mode, where the switches T_m are off, and switches T_x are on, the SM capacitor is connected to terminal AB, in which case $V_{AB} = V_{SM}$. In idle mode, when both switches T_m and T_x are off, the SM terminal is open-circuit and prevents current flow through the SM terminals [3].

The FB-SM has only two switching states, bypass, and insertion, as shown in Fig. 19(b). When the switches T_1 and T_3 are on, and T_2 and T_4 are off, or vice versa, a short circuit occurs, and the SM capacitor is bypassed ($V_{AB} = 0$). Now, if the switches T_1 and T_4 are on, and T_2 and T_3 are off, the positive voltage of the capacitor appears in terminal AB ($V_{AB} = +V_{SM}$). If the switches T_1 and T_4 are off, and T_2 and T_3 are on, the capacitor voltage with reverse polarity appears in terminal AB ($V_{AB} = -V_{SM}$) [3].

HB-SM has half of the FB-SM semiconductor switches, but FB-SM can generate reverse polarity voltage at SM terminals, which can block DC fault current in HVDC [3].

2. Phase-leg MMC-Based PGs

Even though MMC structures suffer from disadvantages such as essential SM capacitor voltage balancing, the need for an HVDC input, and large footprint, the main features of MMC such as modularity, redundancy, scalability of input and output voltage levels, an inherent capacitor in each MMC-SM, etc. has promoted this structure in pulsed power applications [3].

An example of a phase-leg MMC-based PG is shown in Fig. 20(a), fed from the HVDC input. This structure has disadvantages and limitations, which we will address below. The pulses generated by this structure are bipolar by default. If unipolar pulses are needed, the reference point must be transmitted to the ground, i.e., it requires a physical change in the power hardware. Also, the amplitude of generated pulse peak voltage is half of the input HVDC. In this structure, we need two bulky capacitors to create $\pm \frac{1}{2} V_s$ with a mid-point connection [3].

Sensor-based voltage balancing techniques require many measurements, which increases the complexity of the system. Also, high *dv/dt* during switching can cause Electromagnetic Interference (EMI), which may reduce the accuracy of the measured signals [70].

In [71] and [72], by adding a diode between adjacent HB-SM, the voltage of the capacitors is balanced when using a specific switching sequence.

In [71], the capacitors are charged in series from the HVDC power supply to a fraction of the input voltage, and their voltage is balanced in parallel. There is no need to measure the voltage of each capacitor using the Vector Decision Diode (VDD) algorithm.

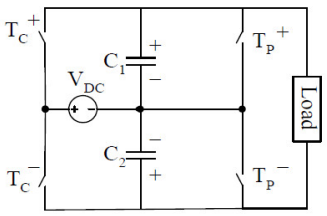

FIGURE 18. **Basic structure of the proposed bipolar PG in [9].**

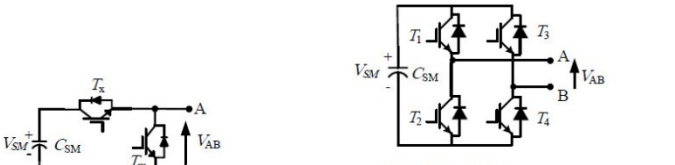

SM Switch States

T_m	T_x	V_{AB}	State
ON	OFF	0	Bypassed
OFF	ON	+ V_{SM}	Inserted
OFF	OFF	Idled	

(a)

FB-SM Switch States

T_1	T_2	T_3	T_4	V_{AB}	State
ON	OFF	ON	OFF	0	Bypassed
OFF	ON	OFF	ON	0	
ON	OFF	OFF	ON	+ V_{SM}	Inserted
OFF	ON	ON	OFF	- V_{SM}	

(b)

FIGURE 19. **Structure of MMC-SMs (a) HB-SM. (b) FB-SM [3].**

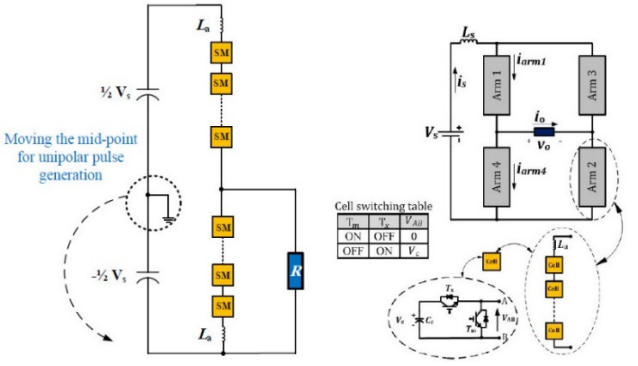

(a) (b)

FIGURE 20. **MMC structures. (a) Phase-leg MMC based PG [3], [71]. (b) MMC based PG presented in [2].**

In [72], the voltage balance of capacitors is provided without complex algorithms and parameter measurements. An inverter with a control current drives the switches to ensure galvanic isolation between the control and power circuits. This structure offers seven levels of unipolar and bipolar output.

In some literature, stacked cells with additional diodes are used to balance the capacitor voltages, which increases the cost of the system. However, in [70], the Phase Disposition Pulse Width Modulation (PDPWM) technique is used, which reduces the cost, complexity, and sensitivity of the system. Due to the high *dv/dt*, the effect of the generated EMI on the system performance is reduced because it does not use voltage and current measurement boards.

In [2], the series connection of MMC-HBs in four arms is used, which together form an H-Bridge, as shown in Fig. 20(b). Each arm contains an inductor L_a to suppress the inrush current between the cell capacitors during their insertion. Arm 3 and Arm 4 are responsible for generating a positive pulse, and Arm 1 and Arm 2 are responsible for generating a negative pulse. Due to the small capacitance of the cells, the dimensions of this structure have been significantly reduced compared to the MMC converter in HVDC transmission applications. The charge and discharge pattern of cell capacitors is such that there is no need for voltage measurement or intricate control to ensure the voltage balance of the capacitors. This structure can produce unipolar and bipolar HV pulses with high-frequency speed.

The topology proposed in [73] is the same structure [2] in terms of hardware, but with the difference that the controller software allows two types of operations, namely: Sensorless mode and sensor-based mode (multilevel mode). In this way, the sensorless mode generates rectangular pulses, while the sensor-based mode can generate different pulses, such as ramp and multipulse. In fact, in this topology, a specific polarity duration can be changed. The default pulses are bipolar, while unipolar pulses can be generated by removing each polarity during pulse generation.

The topology presented in [74] consists of two transition arms with two bi-state arms that form an H-bridge, as shown in Fig. 21. Transition arms, i.e., Arm 1 and Arm 2 (upper arms), are composed of the series connections of MMC-HB

cells that are responsible for generating negative and positive pulses, respectively. Bi-state arms, i.e., Arm 3 and Arm 4 (lower arms), are composed of the series connection of IGBT switches that allow the cells capacitor to be charged. These switches only turn on/off when the arm voltage is zero or near zero, i.e., Zero Voltage Switching (ZVS). This topology can reduce the EMI produced by the converter due to its controllable *dv/dt*. The output waveform of this topology can be rectangular, ramp, and multipulse, in the form of unipolar or bipolar.

As shown in Fig. 22, the topology presented in [75], has two parts called charging system and discharging system. The charging system includes DC power supply, the current limiting resistance R_a, the semiconductor switch T_{2n+1}, capacitors $C_1 - C_{2n}$, voltage equalizing resistances $R_1 - R_{2n}$. The discharging system includes the semiconductor switches $T_1 - T_{2n}$, the diodes $D_1 - D_{2n}$, and the load. The discharging system has two parts, the positive arm (red frame) and the negative arm (blue frame). The resistors $R_1 - R_{2n}$ are very large, but not with large energy losses due to relatively short charging time. This structure can produce a maximum output voltage of $\pm 500V$ with $1KV$ DC voltage source (The voltage amplitude of output pulse is approximately half of the input DC charging voltage.). In addition to the rectangular waveform, exponential and multipulse pulses can be generated by changing the switch's timing.

For a comparative study between the expressed MMC structures, Tables III and IV have been collected. MMC structures require HVDC input, and the output pulse peak is equal to input HVDC, as shown in Table III. All three topologies generate two types of polarity at their output. The topology in [2] generates only rectangular outputs, while the topologies in [73] and [74] also generate different multilevel outputs.

Table IV compares these topologies based on the number of elements. According to Table IV, the number of elements in [2] and [73] is the same because they are the same in terms of hardware, but the topology [74] requires fewer capacitors and inductors. The topology in [74] requires two arms with a series connection of switches, which is one of its disadvantages.

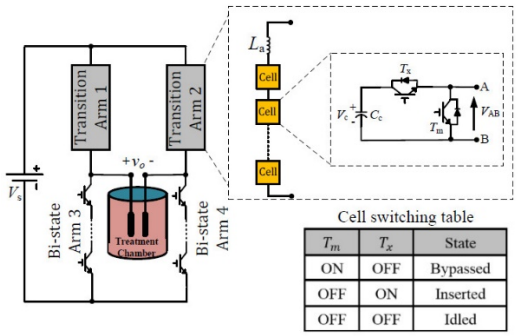

Cell switching table

T_m	T_x	State
ON	OFF	Bypassed
OFF	ON	Inserted
OFF	OFF	Idled

FIGURE 21. **MMC-based PG presented in [74].**

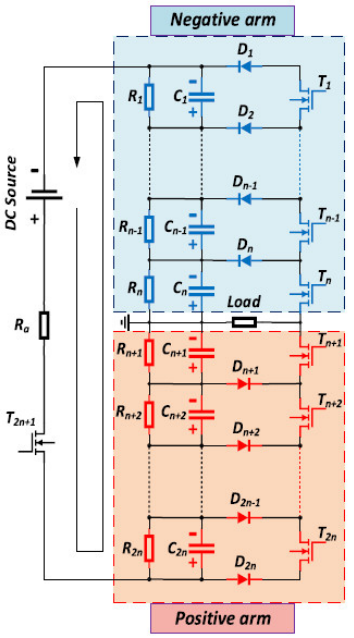

FIGURE 22. **Topology presented in [75].**

TABLE III
COMPARATIVE STUDY BETWEEN MMC-BASED STRUCTURES CONCERNING OUTPUT PULSE CHARACTERISTICS

Topology	Input voltage	Output voltage	Pulse polarity	Pulse shape
[2]	V_{in} (HVDC)	$V_o = V_{in}$	Unipolar/Bipolar	Rectangular
[73]	V_{in} (HVDC)	$V_o = V_{in}$	Unipolar/Bipolar	Rectangular Ramp Multipulse Multilevel
[74]	V_{in} (HVDC)	$V_o = V_{in}$	Unipolar/Bipolar	Rectangular Ramp Multipulse Multilevel

TABLE IV
COMPARATIVE STUDY BETWEEN MMC-BASED STRUCTURES BASED ON THE NUMBER OF ELEMENTS (X : SERIES CONNECTION OF SWITCHES)

Topology	[2]	[73]	[74]
No. of arms	4	4	4
No. of cells per arm	N	N	N
SM type	HB	HB	HB
No. of capacitors	$4N$	$4N$	$2N$
No. of switches	$8N$	$8N$	$4N+2X$
No. of inductors	5	5	2
Other features	Modular Redundancy Scalability	Modular Redundancy Scalability	Modular Redundancy Scalability

C. Hybrid PG Topologies

Non-MMC-based PGs require an HV switch to chop the voltage and are facing the potential challenges of series connections of switches. MMC-based PGs have reduced the need for HV switches and their series connection but suffer

from limitations such as HVDC input. Also, phase-leg MMC-based PGs can only generate bipolar pulses with a voltage amplitude of half the input HVDC. To overcome these limitations, hybrid PGs were introduced, which are fed from the LVDC input and use a voltage boosting mechanism. MMC-SM can be used in the HV pulse generation stage or the voltage boosting stage, or in both stages. Hence, this structure takes advantage of MMC characteristics including modularity, redundancy, and scalability [3].

Hybrid PGs can be divided into two main groups, namely: Non-transformer isolated and transformer isolated.

1. Non-Transformer Isolated Hybrid PGs

In some structures, converters such as Boost, Buck-Boost, and Switched-Capacitive (SC) converter are used to boost the voltage. The Buck-Boost converter is used for smooth start-up from an uncontrolled or fixed DC source. The Boost converter has a wider control range than the Buck-Boost converter and fewer stress on the input switches [51].

In [76], two arms with a series connection of MMC-HB-SMs are used. The capacitors of the SM are charged sequentially via a resistive-inductive (rL) branch and reverse blocking switch (S1 or S2) from an LVDC source, which causes the current to flow under controlled damping, and the capacitors charge rapidly. Hence it can produce pulses with high repetition rates. Arm 1 (upper) is responsible for generating a positive pulse, and Arm 2 (lower) is responsible for generating a negative pulse. The reverse blocking switches turn on by ZVS and turned off by Zero Current Switching (ZCS). The duration and amplitude of the pulse peak are controllable and do not require a voltage sensor. The structure of this PG is shown in Fig. 23.

The structure presented in [77] is the same in [76], except that instead of the rL branch, only L is used, and a series connection of diodes in reverse blocking switches is used because these two switches are exposed to reverse HV during pulse generation. There is no need for a voltage sensor to generate rectangular pulses. Still, due to different capacitance, voltage sensors must be used to generate multilevel waveforms to prevent the capacitor voltage drift. A new voltage balancing technique to overcome capacitor voltage drift uses only one voltage sensor in each MMC-HB arm. This structure requires a fast controller.

The proposed topology in [23] has three main parts: Boost converter, upper arm, and lower arm, as shown in Fig. 24. The Boost converter is powered by the LV input. Two identical switches are used in the Boost converter to reduce the current rating of the switches and charge faster. The upper and lower arms are composed of a series connection of MMC-HB-SMs, the upper arm is responsible for generating positive pulses, and the lower arm is responsible for generating negative pulses. In this topology, capacitors are charged sequentially. Directing/Blocking diodes conduct current from the Boost converter to the capacitors during charging and prevent current flow from the capacitors to the Boost converter. Only one voltage sensor is used to measure the capacitor voltage of the first SM to control the duty ratio of the Boost converter; thus the capacitor voltage of all SMs is controlled.

In [78], the CDVM centrally supplied by a Boost converter, is used to increase the voltage of the LVDC input source, as shown in Fig. 25. Also, the CDVM provides two DC link voltages for the MMC without the need for additional DC link capacitors. Then, the MMC converter generates bipolar and unipolar output voltages when the selector switch is in position (A) or (B), respectively. This structure achieves HV gain with the help of relatively LV devices without the need for a series connection of switches.

In [79], the SC converter is used in the input source to increase the LVDC source voltage. Also, cascaded H-bridges have been used to generate bipolar pulses. A unidirectional switch S_P with a diode D_P is used between the SC converter and the H-Bridges to isolate the load from the input source during pulse generation. This topology can generate nanosecond unipolar and bipolar pulses with ultra-fast dv/dt, as it uses silicon carbide Metal–Oxide Semiconductor Field Effect Transistor (MOSFET) switches. The structure of this PG is shown in Fig. 26. According to the structure of SC, each H-Bridge capacitor can be charged up to $2V_{in}$.

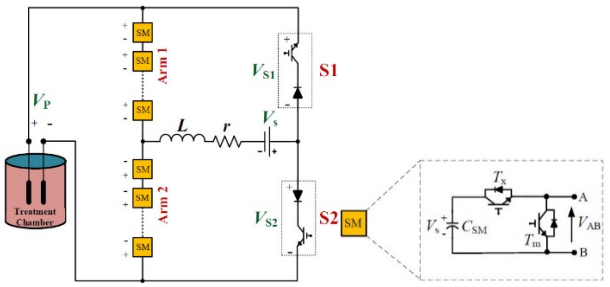

FIGURE 23. Hybrid PG with rL branch presented in [76].

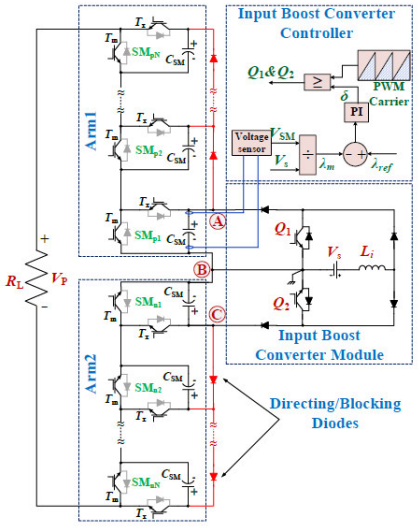

FIGURE 24. Hybrid PG using Boost converter and MMC-SM presented in [23].

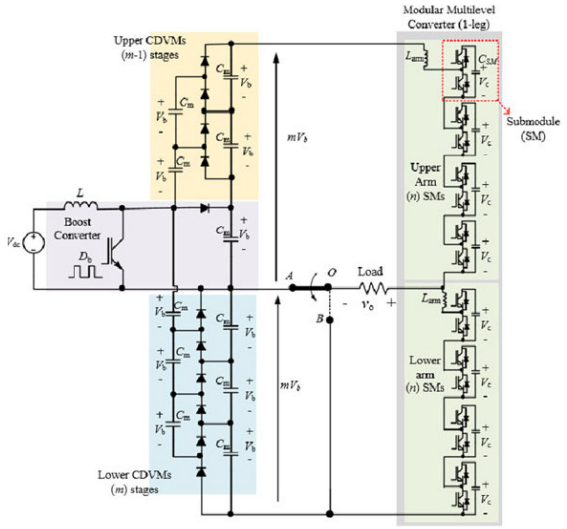

FIGURE 25. Hybrid PG using Boost converter and CDVM to feed phase-leg MMC [78].

In [80], the Boost converter is used to charge the capacitors of the solid-state Marx PG so that the capacitors can be charged to a higher voltage from the input source. The capacitors are charged in parallel, then discharged in series across the load to transfer a large amount of instantaneous power to the load. This modular structure generates unipolar and bipolar pulses with a flexible pattern. It is possible to adjust the pulse width for each positive and negative pulses or both with a change in pulse amplitude. In [81], bipolar pulses can be generated on resistive and resistive-capacitive ($R-C$) loads. The hardware structure of these two topologies is shown in Fig. 27.

In [82], two types of structures are presented, as shown in Fig. 28. In the first structure (Fig. 28(a)), the load resistance acts as the charging resistance of the capacitors, and due to its large size, it is suitable for low repetitive pulse rate applications. In the second structure (Fig. 28(b)), the load resistance is bypassed during charging by a bypass switch, which is a diode. It uses an external limiting resistor, making this structure suitable for high repetitive pulse rate applications. In both structures, there is an arm of a series connection of MMC-HB-SMs. By turning on the switch S_y and the SM switching sequence, the capacitors are charged sequentially. After charging the capacitors, the switch S_y turns off, and the switches S_x and S_{cdi} turn on to discharge the capacitors. In the first structure, a constant voltage DC source can be easily used because the high resistance of the load during charging causes the current spikes to be damped. Still, in the second structure, the power supply voltage must be increased gradually from zero volts during startup, to avoid current surges on switches, because the charging resistance is small. The output of both structures is unipolar.

In [83], [84] solutions for generating bipolar pulses are proposed. In [83], FB-SM has replaced HB-SM to generate bipolar pulses. Also, a thyristor is used instead of a diode to bypass the load during sequential charging of capacitors, as they are available at higher voltage rating and lower conductivity losses compared with self-commutated devices. In addition, thyristors have natural commutation and an inherent reverse voltage blocking capability. In [84], two series arms are used, each arm including a series connection of HB-SMs, one arm generates positive pulses, and the other arm generates negative pulses, as shown in Fig. 29. The H-bridge is used at the input source side to obtain a positive or negative charge voltage, and the capacitors are charged sequentially by this positive or negative voltage. A bidirectional switch such as back-to-back thyristors is used to bypass the load during sequential charging of capacitors.

To compare the Non-transformer isolated Hybrid PGs presented in this paper, Tables V and VI have been collected. Table V is a comparative study of the number of elements used in each relevant structure. According to this table, most structures use MMC-HB-SMs. The topology in [82] requires the least number of capacitors and switches, and the topology in [78] has the highest number of capacitors because it uses a CDVM converter for voltage boosting. Topologies in [79], [82], [83], and [84] do not require an inductor to increase the voltage, while topology in [78] uses the most significant number of inductors. Topologies in [83], [84], in addition to charging resistance, require a thyristor with a voltage rating at the output pulse level.

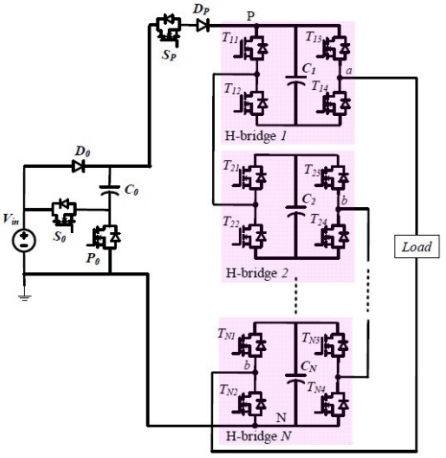

FIGURE 26. Hybrid PG using SC converter and cascaded H-Bridges [79].

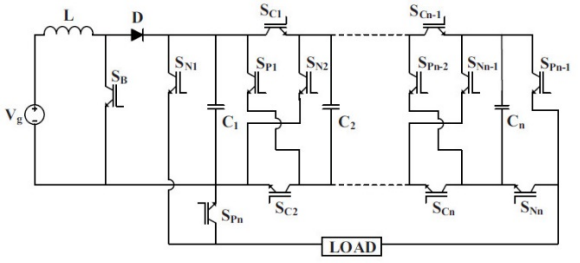

FIGURE 27. Hybrid PG using SMPG concept and Boost converter [80], [81].

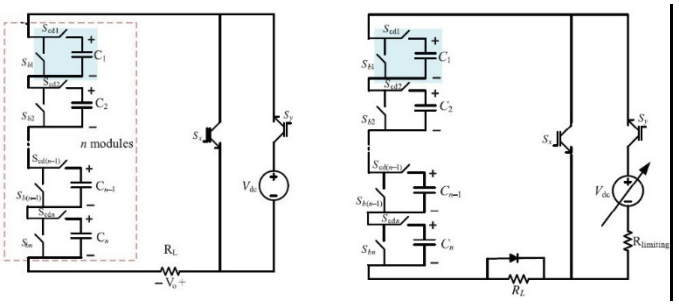

FIGURE 28. Hybrid PG with sequential charging of MMC-HB-SM capacitors. (a) Low repetitive rate. (b) High repetitive rate [82].

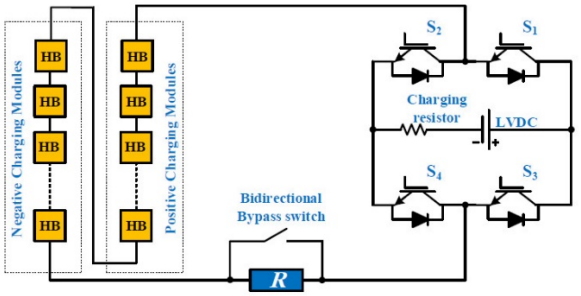

FIGURE 29. Hybrid PG using two MMC-HB-SM series arms to generate positive and negative pulses with H-Bridge at the input power supply [3], [84].

TABLE V

COMPARATIVE STUDY BETWEEN NON-TRANSFORMER ISOLATED HYBRID PGS BASED ON THE NUMBER OF ELEMENTS (X : SERIES CONNECTION OF DIODES, R_{limit} : CHARGING RESISTANCE, LRR: LOW REPETITIVE RATE, HRR: HIGH REPETITIVE RATE AND m : NUMBER OF CDVM STAGES)

Topology	No. of arms	No. of cells per arm	SM type	No. of capacitors	No. of diodes	No. of switches	No. of inductors	Other elements
[76]	2	N	HB	$2N$	2	$4N$+2	1	R_{limit}
[77]	2	N	HB	$2N$	$2X$	$4N$+2	1	-
[23]	2	N	HB	$2N$	$2N$+2	$4N$+2	1	-
[82] LRR	1	N	HB	N	0	$2N$+2	0	R_{load} as R_{limit}
[82] HRR	1	N	HB	N	1	$2N$+2	0	R_{limit}
[78]	2	N	HB	$2N$+4m-1	4m-1	$4N$+1	3	Selector switch
[79]	1	N	FB	N+1	2	$4N$+3	0	-
[80], [81]	-	N	-	N	1	$4N$+1	1	-
[83]	1	N	FB	N	0	$4N$+2	0	R_{limit} and thyristor
[84]	2	N	HB	$2N$	0	$4N$+4	0	R_{limit} and 2*thyristor

TABLE VI

COMPARISON OF NON-TRANSFORMER ISOLATED HYBRID STRUCTURES CONCERNING OUTPUT PULSE CHARACTERISTICS (λ : VOLTAGE BOOSTING FACTOR, m : NUMBER OF CDVM STAGES, D_b : BOOST CONVERTER DUTY CYCLE, d_1 : CHARGING TIME OF BOOST INDUCTOR, R : RESISTIVE LOAD, T : OUTPUT PULSE PERIOD, L : BOOST CONVERTER INDUCTANCE AND d_4 : TOTAL PULSE-WIDTH OF THE BIPOLAR PULSE)

Topology	Input voltage	Output voltage	Pulse polarity	Pulse shape
[76]	V_{in} (LVDC)	NV_{in}	Unipolar/ Bipolar	Rectangular
[77]	V_{in} (LVDC)	λNV_{in}	Unipolar/ Bipolar	Rectangular Multilevel (sensor)
[23]	V_{in} (LVDC)	λNV_{in}	Unipolar/ Bipolar	Rectangular Ramp Multipulse
[82]	V_{in} (LVDC)	NV_{in}	Unipolar	Rectangular
[78]	V_{in} (LVDC)	Unipolar: $\frac{2mV_{in}}{1-D_b}$ Bipolar: $\frac{mV_{in}}{1-D_b}$	Unipolar/ Bipolar	Rectangular
[79]	V_{in} (LVDC)	$2NV_{in}$	Unipolar/ Bipolar	Rectangular
[80], [81]	V_{in} (LVDC)	$\frac{V_{in}}{2}\left(N+\sqrt{N^2+\frac{2d_1^2RT}{Ld_4}}\right)$	Unipolar/ Bipolar	Rectangular
[83]	V_{in} (LVDC)	NV_{in}	Unipolar/ Bipolar	Rectangular Multilevel
[84]	V_{in} (LVDC)	NV_{in}	Unipolar/ Bipolar	Rectangular

Table VI compares the Non-transformer isolated Hybrid PGs in terms of voltage gain and the shape and polarity of the output pulses. All topologies require LVDC inputs, which refers to the nature of their Hybrid, and generate both unipolar and bipolar outputs, except topology in [82], which can only generate unipolar output. Most topologies have

NV_{in} voltage gain, but in the meantime, voltage gain of [79] is $2NV_{in}$ (due to the use of an SC converter), and the voltage gain of [23] and [77] is equal to λNV_{in} (due to the use of a Boost converter). Voltage gain in [78]-[81] has other parameters that must be considered in the calculations. In terms of the output waveform, [23] has shown the best performance to generate three types of waveforms.

2. Transformer Isolated Hybrid PGs

In transformer Isolated Hybrid PGs, transformers are used to increase the voltage, which is generally nanocrystalline cores.

a. Nanocrystalline Transformer Hybrid PGs

Nanocrystalline materials are superior to ferrite due to their high core permeability and have properties such as high magnetizing inductance, near square hysteresis loop, high flux density, etc. [85].

In [86], four stages are used to generate pulses. In the first stage, an H-bridge converts the LVDC source voltage to a high-frequency square ac voltage, as shown in Fig. 30. In the second stage, several nanocrystalline core-based high-frequency step-up transformers with the same turns ratio (1:n) are used to increase the ac voltage level of the first stage. In the third stage, a diode FB rectifier converts the transformer secondary ac square voltage to DC voltage. In the fourth stage, series connections of FB-SMs are used to generate positive or negative output pulses. Each FB-SM capacitor has a dedicated self-regulating charging circuit and does not require sensor-based or sensorless voltage balancing techniques.

In [87], several Voltage Boosting Modules (VBMs) are used at the input power supply side and two series connections of MMC-SM arms at the load side. VBMs use Input-Parallel/ Output-Series and are isolated by nanocrystalline core-based transformers. Arm 1 is an HB-SM, and Arm 2 combines a switch, a capacitor, and two diodes. Depending on the number of utilized VBMs, the turns ratios of the step-up isolation transformers, and the voltage conversion ratio of the individual VBM, the HV pulse can be achieved. This structure does not require a voltage sensor and produces unipolar pulses. If bipolar pulses are needed, two additional MMC arms can be used in the output load. This topology is shown in Fig. 31.

To understand the difference between the two transformer isolated-based structures presented, refer to Table VII. According to Table VII, we find that the topology in [86] has a much better performance in terms of polarity and output waveform than the topology in [87]; in addition, it has fewer capacitors and inductors. But the topology in [87] achieves a higher voltage gain.

TABLE VII
COMPARISON OF HYBRID PGS WITH NANOCRYSTALLINE TRANSFORMERS (n : NUMBER OF SECONDARY TURNS AND D : VBM DUTY RATIO)

Topology	[86]	[87]
No. of modules	N	N : Number of VBM modules p : Number of modules in Arm 1 q : Number of modules in Arm 2
No. of capacitors	N	$2N+p+q$
No. of diodes	$4N$	$N+q$
No. of switches	$4N+4$	$N+2p+q$
No. of inductors	1	N
No. of transformers	N	N
Input voltage	V_{in}	V_{in}
Output voltage	nV_{in}	$\left(\frac{nN}{1-D}\right)V_{in}$
Pulse polarity	Bipolar	Unipolar
Pulse shape	Rectangular Ramp Multilevel	Rectangular

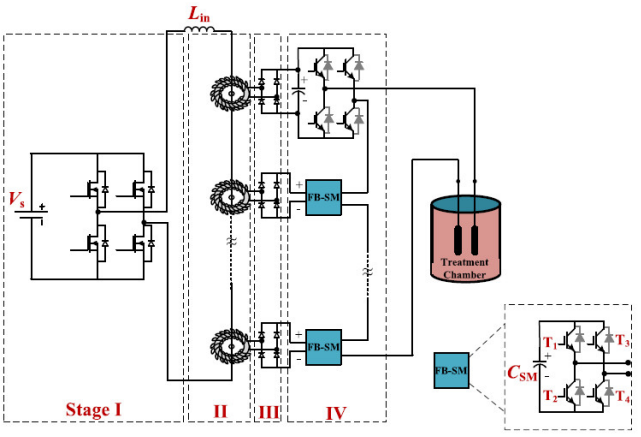

FIGURE 30. Hybrid PG with nanocrystalline core-based transformer and FB-SM [86].

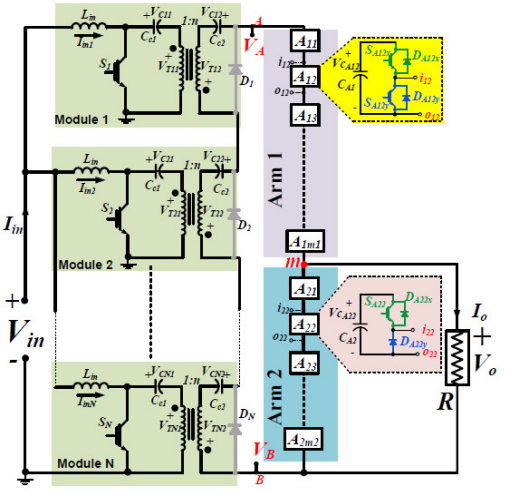

FIGURE 31. Hybrid PG with nanocrystalline core-based transformer and VBMs [87].

b. Resonant Charging Method Transformer Hybrid PGs

Because the number of switches is a significant index of the overall structure, an increase in switches means an increase in driving circuits, protection circuits, and control signals, that leading to a larger and more complex whole structure. The topology presented in [88] is consisting of a special FB module and several HB modules, as shown in Fig. 32. The FB pulse adder can generate the arbitrary waveform output by controlling the timing, while the HB pulse adder has less numbers of switches than the latter. For this reason, in this paper, the HB module is used as the main body of the structure and a specially changed FB module is used to achieve the arbitrary waveform. A capacitor has been added to the conventional FB module to make the same number of charging capacitors as the HB module. Two capacitors have been added to the HB module circuit, which by combining with the special FB module can increase the number of output levels without increasing the number of switches. Multiple HB modules in series can produce an output voltage of 0 or bipolar even-level voltage. By adding the special FB module to multiple HB modules in series, output odd-level voltage can be produced, it means that all levels voltage could be got. The high-frequency resonant charging is selected. Due to the resonant charging method, the charging proceeding is always running, therefore, even with different discharge times of capacitors in a cycle, the output levels will not be inhomogeneity. This structure is simple and compact, and the control technique is flexible. With the same number of output levels, the number of semiconductor switches is significantly reduced. Regardless of the number of HB modules used, this structure can produce $2n$+1 output levels with n+3 switches. The voltage amplitude, frequency, polarity, duration of single pulse, and shape are adjustable. This topology can generate bipolar rectangular, multipulse, step, and multilevel waveforms.

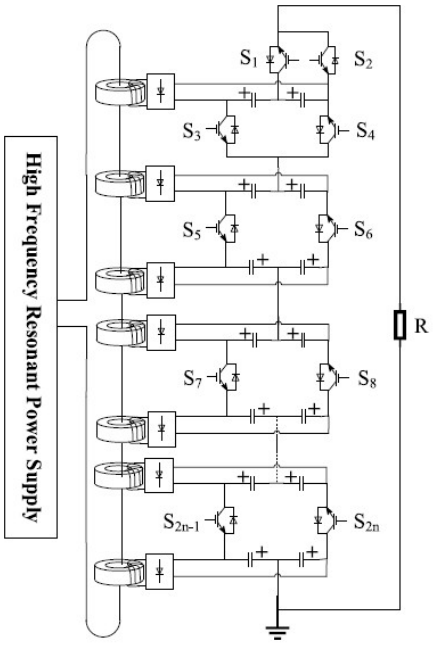

FIGURE 32. Bipolar HB and Special FB resonant charging topology in [88].

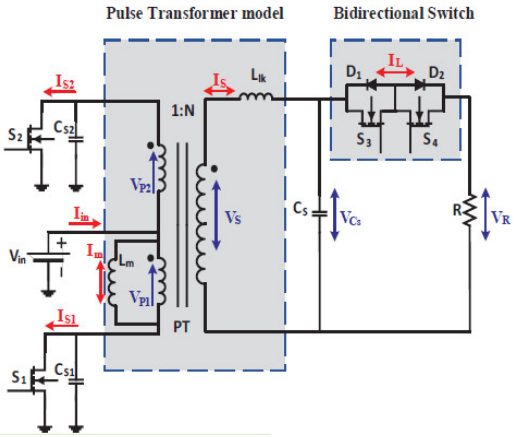

FIGURE 33. Resonance charging technique topology in [45].

Topology presented in [45] has two parts of charging and discharging circuit, as shown in Fig. 33. The LVDC power supply feeds the charging circuit. The charging part has a push-pull converter and the push-pull transformer is responsible for providing isolation between the power supply and the load. The transformer turn ratio is selected $1/1/N$, which increases the voltage gain by N. Hence, the capacitor is charged more than NV_{in}. The lower part of the charging circuit includes the DC voltage source and a transformer winding, the lower part and the upper part are responsible for generating positive and negative pulses, respectively. C_{s1} and C_{s2} are snubber capacitors that are responsible to reset the transformer core to provide the proper condition for next cycles. These capacitors figure a resonant circuit with L_m and V_{in}. On the secondary side are only resonance charging elements such as leakage inductance of transformer (as a virtual inductor) and one capacitor. This causes the capacitor to be charged with higher gain. The capacitor C_s and the inductance L_{lk} together figure a resonant circuit. Hence, the capacitor C_s is charged twice of the voltage of $V_{\sec}$. Switches S_3 and S_4 (bidirectional switch) are responsible for generating positive and negative pulses, respectively. This bidirectional switch can produce a regulated bipolar voltage with a very simple fixed frequency control. The presence of a transformer as well as the resonance between the leakage inductance of the transformer and the capacitor leads to an increase in voltage gain, which will reduce the required charging elements. Using two windings on the primary side causes bias voltage for the bipolar pulses. To generate unipolar pulses, one of the primary side switches must be turned off. This structure has the advantages of ease of switching controlling design, increase the gain, sensor-less configuration and with low elements to produce bipolar pulses, which leads to a cost and size effective structure.

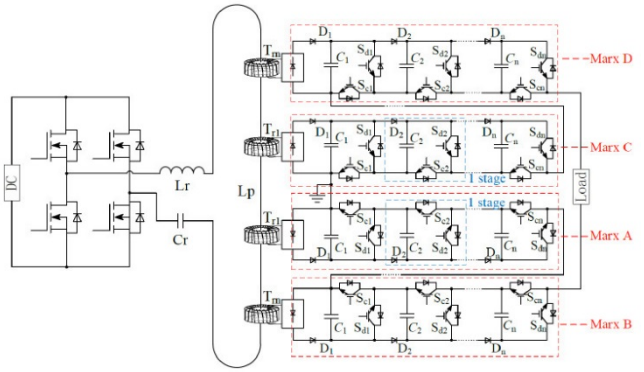

FIGURE 34. Multistage resonant charging bipolar Marx generator presented in [89].

One way to increase the output voltage pulse is to increase the number of stages of the Marx generator, but this will cause energy loss and stability problems. To solve these problems, as shown in Fig. 34, in [89] the full bridge resonant charging method is adopted in combination with the topology presented in [90]. This Marx generator uses high frequency resonant charging. This structure includes a dc power supply, a full-bridge series resonant circuit, six eight-stage Marx generators, and a driving circuit. Marx generator capacitors are charged in parallel simultaneously via the Pulse Transformers (PTs) by the resonant power supply and discharged in series on the load. PTs transmit controlling signal and power simultaneously and prevent short-circuit fault (magnetic insulation). The elements L_r and C_r are resonant inductance (leakage inductance) and resonant capacitor, respectively. A and B are positive-pulse Marx generators, and C and D are negative-pulse Marx generators. The last capacitor of Marx generator A (C) is connected to the first capacitor of Marx generator B (D). To solve the problem of charging voltage imbalance between each Marx generator, which is due to the parameter difference between the PT magnetic cores, equalizing winding has been used, which can reduce the surge current between each stage. By setting the switching frequency to half the resonant frequency, the soft-switching state will be achieved. As the switching frequency increases, the volume of the magnetic cores decreases, leading to a more compact structure. The saturation of the magnetic core limits the pulse width, hence, the half-bridge driving circuit is used. The charging source and discharge circuit are electrically insulated and relatively independent. By comparing the multistage resonant charging method with the dc constant voltage charging method (used in solid-state Marx generators), the delivery of the former is higher than the latter. This structure has advantages such as better performance than traditional solid-state generator (by increasing the number of stages), easiness of integration, reliable and stable operation and higher power density. This structure untangled the problem of surge current and voltage drop of the article presented in [90].

IV. COMPARISON STUDY BETWEEN POWER ELECTRONICS-BASED PULSE GENERATORS SUBGROUPS

As mentioned before, to create IRE, HV pulses with particular specifications in terms of the waveform, voltage amplitude, pulse width, etc., are needed. To generate these pulses, we must use a pulse generator device. By studying this paper, we figured out that PGs can be divided into two main groups, namely: classical PGs and power electronics-based PGs. Power electronics-based PGs are also divided into three subgroups, namely: Non-MMC based, MMC-based, and Hybrid. These three subgroups of power electronics-based PGs are compared in Table VIII, and some of their main features and limitations are described.

TABLE VIII
COMPARISON BETWEEN THREE MAIN GROUPS OF POWER ELECTRONICS-BASED PGS [3]

	Non-MMC	MMC	Hybrid
Ref.	[48]-[51], [57]-[61], [64], [67], [68]	[71]-[72]	[78], [82]-[84]
Features	*Simple control *LVDC supply fed *No voltage sensors *Small footprint	*Modular *Scalable *Redundant *Generate different pulse waveforms *Reduced semiconductor ratings	*No HV switches for HVDC chopping *LVDC supply fed *In order to form pulses, MMC modules are connected across the load *Moderate footprint
Limitations	*Requires HV switches *Lacks modularity *Inflexible pulse characterizations *Parameter change sensitivity *Generated pulses, mainly rectangular	*Indispensable SM capacitor voltage balancing *HVDC supply fed *Complex control with the sensorless performance (feasibly) *Large footprint	*To avoid capacitor voltage drift, sensors are needed *If SM capacitors are charged separately, various pulse waveforms reached, else drift in HV levels

V. CONCLUSIONS AND FUTURE DIRECTIONS

The electroporation process, its types, and applications were explained in this article. A general classification of pulse generators was introduced, namely: classical pulse generators and power electronics-based pulse generators. Classical pulse generators use spark gaps and gas switches, while power electronics-based pulse generators use power electronics switches due to high voltage tolerate and quick on/off switching performance. Several topologies from different works of literature have been presented from each group and subgroup. In addition, a comparative study between these groups, as well as the topologies of each subgroup, has been provided. Designing and developing HV pulse generators suitable for electroporation is a challenging

task due to the tight requirements of isolation, controllability, reliability, voltage amplitude and output impedance.

According to what we learned in this review article, some recommendations and suggestions for future research and further research work can be made: 1) replacing the Si IGBTs used in MMC-SM with wide band gap semiconductor devices such as silicon-carbide and gallium nitride (higher voltage, sub-microsecond pulse durations, and fast repetition rates), 2) the need for re-modelling the electroporation load when using wide band gap devices (for pulses with sub-microsecond duration, ignoring the load capacitance will not be valid), 3) investigating the effects of electrode geometry and shape on electric field distribution and pulsed power performance using Finite Element simulations, and 4) evaluation of efficiency and productivity of applications. At this point in time, gallium nitride-based technology is cost-effective that challenges silicon, and gallium nitride could have the most potential in taking down silicon.

The brilliant future of electroporation technology requires the development of versatile generators that overcome all current limitations and provide a useful device for research and applications.

REFERENCES

[1] O. Lucia, H. Sarnago, T. Garcia-Sanchez, L. M. Mir, and J. M. Burdio, "Industrial Electronics for Biomedicine: A New Cancer Treatment Using Electroporation," *IEEE Ind. Electron. Mag.*, vol. 13, no. 4, pp. 6–18, Dec. 2019, doi: 10.1109/MIE.2019.2942377.

[2] M. A. Elgenedy, A. Darwish, S. Ahmed, and B. W. Williams, "A Modular Multilevel-Based High-Voltage Pulse Generator for Water Disinfection Applications," *IEEE Trans. Plasma Sci.*, vol. 44, no. 11, pp. 2893–2900, Nov. 2016, doi: 10.1109/TPS.2016.2610462.

[3] M. A. Elgenedy, "High-voltage pulse generators incorporating modular multilevel converter sub-modules," Strathclyde University, 2018.

[4] M. A. Elgenedy, A. Massoud, D. Holliday, S. Ahmed, and B. W. Williams, "High-voltage pulse generator using sequentially charged full-bridge modular multilevel converter Sub-modules, for water treatment applications," *J. Eng.*, vol. 2019, no. 17, pp. 4537–4544, Jun. 2019, doi: 10.1049/JOE.2018.8054.

[5] H. Sarnago, O. Lucia, A. Naval, J. M. Burdio, Q. Castellvi, and A. Ivorra, "A Versatile Multilevel Converter Platform for Cancer Treatment Using Irreversible Electroporation," *IEEE J. Emerg. Sel. Top. Power Electron.*, vol. 4, no. 1, pp. 236–242, Mar. 2016, doi: 10.1109/JESTPE.2015.2512324.

[6] P. Davari, "High Frequency High Power Converters for Industrial Applications," Queensland University of Technology, 2013.

[7] H. Akiyama, S. Sakai, T. Sakugawa, and T. Namihira, "Environmental applications of repetitive pulsed power," *IEEE Trans. Dielectr. Electr. Insul.*, vol. 14, no. 4, pp. 825–833, Aug. 2007, doi: 10.1109/TDEI.2007.4286513.

[8] K. Takaki, "Removal of nitric oxide in flue gases by multipoint to plane dielectric barrier discharge," *IEEE Trans. Plasma Sci.*, vol. 27, no. 4, pp. 1137–1145, 1999, doi: 10.1109/27.782294.

[9] M. R. Delshad, M. Rezanejad, and A. Sheikholeslami, "A New Modular Bipolar High-Voltage Pulse Generator," *IEEE Trans. Ind. Electron.*, vol. 64, no. 2, pp. 1195–1203, Feb. 2017, doi: 10.1109/TIE.2016.2611460.

[10] H. Akiyama, T. Sakugawa, T. Namihira, K. Takaki, Y. Minamitani, and N. Shimomura, "Industrial applications of pulsed power technology," *IEEE Trans. Dielectr. Electr. Insul.*, vol. 14, no. 5, pp. 1051–1064, Oct. 2007, doi: 10.1109/TDEI.2007.4339465.

[11] R. Brandenburg *et al.*, "Antimicrobial effects of UV and VUV radiation of nonthermal plasma jets," *IEEE Trans. Plasma Sci.*, vol. 37, no. 6 PART 1, pp. 877–883, 2009, doi: 10.1109/TPS.2009.2019657.

[12] F. Fukawa, N. Shimomura, T. Yano, S. Yamanaka, K. Teranishi, and H. Akiyama, "Application of nanosecond pulsed power to ozone production by streamer corona," *IEEE Trans. Plasma Sci.*, vol. 36, no. 5 PART 3, pp. 2592–2597, 2008, doi: 10.1109/TPS.2008.2004372.

[13] A. Golberg, J. Kandel, M. Belkin, and B. Rubinsky, "Intermittently delivered pulsed electric fields for sterile storage of turbid media," *IEEE Trans. Plasma Sci.*, vol. 38, no. 11 PART 2, pp. 3211–3218, Nov. 2010, doi: 10.1109/TPS.2010.2065246.

[14] T. Matsumoto, D. Wang, T. Namihira, and H. Akiyama, "Energy efficiency improvement of nitric oxide treatment using nanosecond pulsed discharge," *IEEE Trans. Plasma Sci.*, vol. 38, no. 10 PART 1, pp. 2639–2643, Oct. 2010, doi: 10.1109/TPS.2010.2045903.

[15] R. Narsetti, R. D. Curry, K. F. McDonald, L. M. Nichols, and T. Clevenger, "Application of pulsed electric fields and magnetic pulse compressor technology for water sterilization," *Dig. Tech. Pap. Int. Pulsed Power Conf.*, pp. 1282–1285, 2007, doi: 10.1109/PPC.2005.300606.

[16] S. Y. Tseng, T. F. Wu, and Y. M. Chen, "Wide pulse combined with narrow-pulse generator for food sterilization," *IEEE Trans. Ind. Electron.*, vol. 55, no. 2, pp. 741–748, Feb. 2008, doi: 10.1109/TIE.2007.910517.

[17] N. Shimomura *et al.*, "Nanosecond pulsed power application to nitrogen oxides treatment with coaxial reactors," *IEEE Trans. Dielectr. Electr. Insul.*, vol. 18, no. 4, pp. 1274–1280, Aug. 2011, doi: 10.1109/TDEI.2011.5976127.

[18] Y. Matsumoto, N. Shioji, T. Satake, and A. Sakuma, "Inactivation of microorganisms by pulsed high voltage application," pp. 652–659, 1992, doi: 10.1109/IAS.1991.178248.

[19] A. Mizuno and Y. Hori, "Destruction of Living Cells by Pulsed High-Voltage Application," *IEEE Trans. Ind. Appl.*, vol. 24, no. 3, pp. 387–394, 1988, doi: 10.1109/28.2886.

[20] K. Shimizu, M. Blajan, and S. Tatematsu, "Basic study of remote disinfection and sterilization effect by using atmospheric microplasma," *Conf. Rec. - IAS Annu. Meet. (IEEE Ind. Appl. Soc.*, 2011, doi: 10.1109/IAS.2011.6074269.

[21] A. Khavari, Z. Orafa, M. Hashemi, N. Habibzadeh, and A. Bolhassani, "Different physical delivery systems: An important approach for delivery of biological molecules in vivo", Arch Adv Biosci, vol. 7, no. 1, pp. 48-63, Jan. 2016.

[22] M. Reberšek, D. Miklavčič, C. Bertacchini, and M. Sack, "Cell membrane electroporation-Part 3: The equipment," *IEEE Electr. Insul. Mag.*, vol. 30, no. 3, pp. 8–18, 2014, doi: 10.1109/MEI.2014.6804737.

[23] M. A. Elgenedy, A. M. Massoud, S. Ahmed, B. W. Williams, and J. R. McDonald, "A Modular Multilevel Voltage-Boosting Marx Pulse-Waveform Generator for Electroporation Applications," *IEEE Trans. Power Electron.*, vol. 34, no. 11, pp. 10575–10589, Nov. 2019, doi: 10.1109/TPEL.2019.2899974.

[24] H. Bluhm, *Pulsed Power System: Principle and Applications*. Berlin Heidelberg: Springer-Verlag, 2006.

[25] K. R. Prestwich and D. L. Johnson, "Development of an 18-megavolt marx generator," *IEEE Trans. Nucl. Sci.*,

vol. 16, no. 3, pp. 64–69, 1969, doi: 10.1109/TNS.1969.4325179.

[26] R. A. Fitch, "Marx - and marx-like - high-voltage generators," *IEEE Trans. Nucl. Sci.*, vol. 18, no. 4, pp. 190–198, 1971, doi: 10.1109/TNS.1971.4326339.

[27] A. Carrus, "MARX CIRCUIT MODIFIED BY ADDING A TAIL SPHERE GAP TO GENERATE LIGHTNING IMPULSES LASTING A FEW MICROSECONDS.," *IEE Proc. A Phys. Sci. Meas. Instrumentation. Manag. Educ. Rev.*, vol. 132, no. 1 pt A, pp. 40–44, 1985, doi: 10.1049/IP-A-1.1985.0007.

[28] T. Heeren, T. Ueno, D. Wang, T. Namihira, S. Katsuki, and H. Akiyama, "Novel Dual Marx Generator for Microplasma Applications," *IEEE Trans. Plasma Sci.*, vol. 33, no. 4, pp. 1205–1209, 2005, doi: 10.1109/TPS.2005.852433.

[29] A. Rajabi-Nezhad, A. A. Razi-Kazemi, M. Soheyli and F. Malekipour, "Assessment of Different Compact Marx Generator Structures on the Voltage Profile," in IEEE Transactions on Plasma Science, vol. 48, no. 1, pp. 189-195, Jan. 2020, doi: 10.1109/TPS.2019.2955634.

[30] J. Clementson, K. Rahbarnia, O. Grulke, and T. Klinger, "Design of A, B, and C pulse forming networks using the VINPFN application," *IEEE Trans. Power Electron.*, vol. 29, no. 11, pp. 5673–5679, 2014, doi: 10.1109/TPEL.2013.2295245.

[31] S. M. H. Hosseini and H. R. Ghaforinam, "Improving the pulse generator BOOST PFN to increase the amplitude and decrease the pulse duration of the voltage," *IEEE Trans. Dielectr. Electr. Insul.*, vol. 23, no. 3, pp. 1699–1704, Jun. 2016, doi: 10.1109/TDEI.2016.005381.

[32] H. Ghawde and R. Harchandani, "Comparison of pulse forming networks for Marx generator," *2017 Int. Conf. Nascent Technol. Eng. ICNTE 2017 - Proc.*, Jun. 2017, doi: 10.1109/ICNTE.2017.7947939.

[33] S. Mohsenzade, M. Zarghany, M. Aghaei, and S. Kaboli, "A High-Voltage Pulse Generator With Continuously Variable Pulsewidth Based on a Modified PFN," *IEEE Trans. Plasma Sci.*, vol. 45, no. 5, pp. 849–858, May 2017, doi: 10.1109/TPS.2017.2683800.

[34] L. Yu, Y. Feng, T. Sugai, and W. Jiang, "Voltage adding of pulse forming lines using inductive energy storage," *IEEE Trans. Dielectr. Electr. Insul.*, vol. 24, no. 4, pp. 2211–2215, 2017, doi: 10.1109/TDEI.2017.006421.

[35] J. Wu *et al.*, "A novel compact repetitive frequency square-wave generator based on coaxial pulse forming lines and coupled magnetic switches," *IEEE Trans. Plasma Sci.*, vol. 42, no. 6, pp. 1714–1720, 2014, doi: 10.1109/TPS.2014.2322031.

[36] G. H. Rim, E. P. Pavlov, H. S. Lee, J. S. Kim, and Y. W. Choi, "Pulse forming lines for square pulse generators," *IEEE Trans. Plasma Sci.*, vol. 31, no. 2, pp. 196–200, Apr. 2003, doi: 10.1109/TPS.2003.810185.

[37] C. C. Kung, E. A. Chauchard, C. H. Lee, and M. J. Rhee, "Kilovolt Square Pulse Generation by a Dual of the Blumlein Line with a Photoconductive Semiconductor Opening Switch," *IEEE Photonics Technol. Lett.*, vol. 4, no. 6, pp. 621–623, 1992, doi: 10.1109/68.141988.

[38] M. T. Domonkos and J. P. O'Loughlin, "Marxed transmission lines for compact pulsed power," *IEEE Trans. Dielectr. Electr. Insul.*, vol. 20, no. 6, pp. 2350–2354, 2013, doi: 10.1109/TDEI.2013.6678889.

[39] Y. Mi, Y. Zhang, J. Wan, C. Yao, and C. Li, "Nanosecond pulse generator based on an unbalanced blumlein-type multilayered microstrip transmission line and solid-state switches," *IEEE Trans. Plasma Sci.*, vol. 44, no. 5, pp. 795–802, May 2016, doi: 10.1109/TPS.2016.2542521.

[40] G.A.Mesyats, *Pulsed Power*. New York: Kluwer Academic, 2005.

[41] Z. Liu, "Multiple-switch pulsed power generation based on a transmission line transformer," Technische Universiteit Eindhoven, 2008.

[42] J. Choi *et al.*, "Feasibility studies of EMTP simulation for the design of the pulsed-power generator using MPC and BPFN for water treatments," *IEEE Trans. Plasma Sci.*, vol. 34, no. 5 I, pp. 1744–1750, Oct. 2006, doi: 10.1109/TPS.2006.883384.

[43] E. Schamiloglu, R. J. Barker, M. Gundersen, and A. A. Neuber, "Scanning the technology: Modern pulsed power: Charlie Martin and Beyond," *Proc. IEEE*, vol. 92, no. 7, pp. 1014–1019, 2004, doi: 10.1109/JPROC.2004.829058.

[44] S. Zabihi, F. Zare, G. Ledwich, A. Ghosh, and H. Akiyama, "A new family of marx generators based on commutation circuits," *IEEE Trans. Dielectr. Electr. Insul.*, vol. 18, no. 4, pp. 1181–1188, Aug. 2011, doi: 10.1109/TDEI.2011.5976113.

[45] Y. H. Tabrizi, M. Nasir Uddin and H. Allahyari, "A High-Gain Bipolar Pulse Power Generator Employed Bidirectional Switch for Dielectric Barrier Discharge Applications Based on Resonance Charging Technique," 2021 IEEE Industry Applications Society Annual Meeting (IAS), 2021, pp. 1-7, doi: 10.1109/IAS48185.2021.9677367.

[46] J. Rodríguez, S. Bernet, B. Wu, J. O. Pontt, and S. Kouro, "Multilevel voltage-source-converter topologies for industrial medium-voltage drives," *IEEE Trans. Ind. Electron.*, vol. 54, no. 6, pp. 2930–2945, Dec. 2007, doi: 10.1109/TIE.2007.907044.

[47] L. Redondo and J. F. Silva, "Solid State Pulsed Power Electronics," *Power Electron. Handb.*, pp. 669–707, Jan. 2011, doi: 10.1016/B978-0-12-382036-5.00026-4.

[48] E. Veilleux, B. T. Ooi, and P. W. Lehn, "Marx dc-dc converter for high-power application," *IET Power Electron.*, vol. 6, no. 9, pp. 1733–1741, 2013, doi: 10.1049/IET-PEL.2013.0025.

[49] H. Shi, Y. Lu, T. Gu, J. Qiu, and K. Liu, "High-voltage pulse waveform modulator based on solid-state Marx generator," *IEEE Trans. Dielectr. Electr. Insul.*, vol. 22, no. 4, pp. 1983–1990, Aug. 2015, doi: 10.1109/TDEI.2015.004959.

[50] T. Sakamoto, A. Nami, M. Akiyama, and H. Akiyama, "A repetitive solid state marx-type pulsed power generator using multistage switch-capacitor cells," *IEEE Trans. Plasma Sci.*, vol. 40, no. 10 PART 1, pp. 2316–2321, 2012, doi: 10.1109/TPS.2012.2184776.

[51] C. Yao, S. Dong, Y. Zhao, Y. Mi, and C. Li, "A Novel Configuration of Modular Bipolar Pulse Generator Topology Based on Marx Generator with Double Power Charging," *IEEE Trans. Plasma Sci.*, vol. 44, no. 10, pp. 1872–1878, Oct. 2016, doi: 10.1109/TPS.2016.2542103.

[52] C. Yao, X. Zhang, F. Guo, S. Dong, Y. Mi, and C. Sun, "FPGA-controlled all-solid-state nanosecond pulse generator for biological applications," *IEEE Trans. Plasma Sci.*, vol. 40, no. 10 PART 1, pp. 2366–2372, 2012, doi: 10.1109/TPS.2012.2188908.

[53] L. M. Redondo, J. F. Silva, P. Tavares, and E. Margato, "High-voltage high-frequency Marx-bank type pulse generator using integrated power semiconductor half-bridges," *2005 Eur. Conf. Power Electron. Appl.*, vol. 2005, 2005, doi: 10.1109/EPE.2005.219301.

[54] Y. Gu, C. Zhang, W. Bian, S. Wu and Z. Xu, "A Novel Modular Pulse Generator With High Voltage Gain and Reduced Number of Capacitors," in IEEE Transactions on Plasma Science, vol. 50, no. 2, pp. 394-400, Feb. 2022, doi: 10.1109/TPS.2022.3140225.

[55] H. Canacsinh, J. F. Silva, and L. M. Redondo, "Dual resonant voltage droop compensation for bipolar solid-state marx generator topologies," *IEEE Trans. Plasma Sci.*, vol. 47, no. 1, pp. 1017–1023, Jan. 2019, doi: 10.1109/TPS.2018.2868495.

[56] Z. Li, H. Liu, S. Jiang, L. Guo and J. Rao, "A High-Current All-Solid-State Pulse Generator Based on Marx Structure," in IEEE Transactions on Plasma Science, vol.

48, no. 10, pp. 3629-3636, Oct. 2020, doi: 10.1109/TPS.2020.3021197.

[57] A. Elserougi, S. Ahmed, and A. Massoud, "A boost converter-based ringing circuit with high-voltage gain for unipolar pulse generation," *IEEE Trans. Dielectr. Electr. Insul.*, vol. 23, no. 4, pp. 2088–2094, Aug. 2016, doi: 10.1109/TDEI.2016.7556482.

[58] A. Elserougi, A. M. Massoud, and S. Ahmed, "A boost-inverter-based bipolar high-voltage pulse generator," *IEEE Trans. Power Electron.*, vol. 32, no. 4, pp. 2846–2855, Apr. 2017, doi: 10.1109/TPEL.2016.2576562.

[59] S. Zabihi, F. Zare, G. Ledwich, A. Ghosh, and H. Akiyama, "A new pulsed power supply topology based on positive buck-boost converters concept," *IEEE Trans. Dielectr. Electr. Insul.*, vol. 17, no. 6, pp. 1901–1911, Dec. 2010, doi: 10.1109/TDEI.2010.5658245.

[60] S. Zabihi, F. Zare, G. Ledwich, A. Ghosh, and H. Akiyama, "A novel high-voltage pulsed-power supply based on low-voltage switch-capacitor units," *IEEE Trans. Plasma Sci.*, vol. 38, no. 10 PART 2, pp. 2877–2887, Oct. 2010, doi: 10.1109/TPS.2010.2060364.

[61] L. M. Redondo and J. F. Silva, "Flyback versus forward switching power supply topologies for unipolar pulsed-power applications," *IEEE Trans. Plasma Sci.*, vol. 37, no. 1, pp. 171–178, 2009, doi: 10.1109/TPS.2008.2006056.

[62] A. Elserougi, S. Ahmed, and A. Massoud, "High voltage pulse generator based on DC-to-DC boost converter with capacitor-diode voltage multipliers for bacterial decontamination," *IECON 2015 - 41st Annu. Conf. IEEE Ind. Electron. Soc.*, pp. 322–326, 2015, doi: 10.1109/IECON.2015.7392119.

[63] A. Elserougi, S. Ahmed, and A. Massoud, "High-voltage pulse generator based on capacitor-diode voltage multiplier centrally fed from dc-dc boost converter," *IET Conf. Publ.*, vol. 2016, no. CP684, 2016, doi: 10.1049/CP.2016.0278.

[64] A. Elserougi, A. M. Massoud, A. M. Ibrahim, and S. Ahmed, "A high voltage pulse-generator based on DC-to-DC converters and capacitor-diode voltage multipliers for water treatment applications," *IEEE Trans. Dielectr. Electr. Insul.*, vol. 22, no. 6, pp. 3290–3298, Dec. 2015, doi: 10.1109/TDEI.2015.005376.

[65] A. Elserougi, S. Ahmed, and A. Massoud, "Multi-module high voltage pulse generator based on DC-DC boost converter and CDVMs for drinking water purification," *Proc. IEEE Int. Conf. Ind. Technol.*, vol. 2016-May, pp. 334–338, May 2016, doi: 10.1109/ICIT.2016.7474774.

[66] A. A. Elserougi, A. S. Abdel-Khalik, S. Ahmed, and A. M. Massoud, "AC-powered multi-module high-voltage pusle-generator with sinusoidal input current for water treatment via underwater pulsed arc discharge," *2017 11th IEEE Int. Conf. Compat. Power Electron. Power Eng. CPE-POWERENG 2017*, pp. 163–168, Apr. 2017, doi: 10.1109/CPE.2017.7915163.

[67] L. M. Redondo, "A DC voltage-multiplier circuit working as a high-voltage pulse generator," *IEEE Trans. Plasma Sci.*, vol. 38, no. 10 PART 1, pp. 2725–2729, Oct. 2010, doi: 10.1109/TPS.2010.2050495.

[68] M. Rezanejad, A. Sheikholeslami, and J. Adabi, "Modular switched capacitor voltage multiplier topology for pulsed power supply," *IEEE Trans. Dielectr. Electr. Insul.*, vol. 21, no. 2, pp. 635–643, 2014, doi: 10.1109/TDEI.2013.004067.

[69] G. P. Adam, S. J. Finney, A. M. Massoud, and B. W. Williams, "Capacitor balance issues of the diode-clamped multilevel inverter operated in a quasi two-state mode," *IEEE Trans. Ind. Electron.*, vol. 55, no. 8, pp. 3088–3099, 2008, doi: 10.1109/TIE.2008.922607.

[70] A. A. Elserougi, A. M. Massoud, and S. Ahmed, "Modular Multilevel Converter-Based Bipolar High-Voltage Pulse Generator with Sensorless Capacitor Voltage Balancing Technique," *IEEE Trans. Plasma Sci.*, vol. 44, no. 7, pp. 1187–1194, Jul. 2016, doi: 10.1109/TPS.2016.2575861.

[71] L. L. Rocha, J. F. Silva, and L. M. Redondo, "Multilevel high-voltage pulse generation based on a new modular solid-state switch," *IEEE Trans. Plasma Sci.*, vol. 42, no. 10, pp. 2956–2961, Oct. 2014, doi: 10.1109/TPS.2013.2296141.

[72] L. L. Rocha, J. F. Silva, and L. M. Redondo, "Seven-Level Unipolar/Bipolar Pulsed Power Generator," *IEEE Trans. Plasma Sci.*, vol. 44, no. 10, pp. 2060–2064, Oct. 2016, doi: 10.1109/TPS.2016.2519269.

[73] M. A. Elgenedy, A. Darwish, S. Ahmed, and B. W. Williams, "A Modular Multilevel Generic Pulse-Waveform Generator for Pulsed Electric Field Applications," *IEEE Trans. Plasma Sci.*, vol. 45, no. 9, pp. 2527–2535, Sep. 2017, doi: 10.1109/TPS.2017.2727068.

[74] M. A. Elgenedy, A. Darwish, S. Ahmed, and B. W. Williams, "A Transition Arm Modular Multilevel Universal Pulse-Waveform Generator for Electroporation Applications," *IEEE Trans. Power Electron.*, vol. 32, no. 12, pp. 8979–8991, Dec. 2017, doi: 10.1109/TPEL.2017.2653243.

[75] S. Jiang, J. Wang, Y. Wang, Z. Li and J. Rao, "A Multilevel Pulse Generator Based on Series Capacitor Structure for Cell Electroporation," in IEEE Transactions on Plasma Science, vol. 48, no. 12, pp. 4235-4241, Dec. 2020, doi: 10.1109/TPS.2020.3032708.

[76] M. A. Elgenedy, A. M. Massoud, S. Ahmed, and B. W. Williams, "A High-Gain, High-Voltage Pulse Generator Using Sequentially Charged Modular Multilevel Converter Submodules, for Water Disinfection Applications," *IEEE J. Emerg. Sel. Top. Power Electron.*, vol. 6, no. 3, pp. 1394–1406, Sep. 2018, doi: 10.1109/JESTPE.2017.2750244.

[77] M. A. Elgenedy, A. Darwish, S. Ahmed, B. W. Williams, and J. R. McDonald, "High-voltage pulse generator based on sequentially charged MMC-SMs operating in a voltage-boost mode," *IET Power Electron.*, vol. 12, no. 4, pp. 749–758, Apr. 2019, doi: 10.1049/IET-PEL.2018.5438.

[78] A. A. Elserougi, M. Faiter, A. M. Massoud, and S. Ahmed, "A Transformerless Bipolar/Unipolar High-Voltage Pulse Generator with Low-Voltage Components for Water Treatment Applications," *IEEE Trans. Ind. Appl.*, vol. 53, no. 3, pp. 2307–2319, May 2017, doi: 10.1109/TIA.2017.2666080.

[79] M. K. Nguyen, F. Zare, and N. Ghasemi, "Switched-capacitor-based nanosecond pulse generator using SiC MOSFET," *Australas. Univ. Power Eng. Conf. AUPEC 2018*, Nov. 2018, doi: 10.1109/AUPEC.2018.8757883.

[80] D. Malviya and M. Veerachary, "A Novel Boost Converter Based High-Voltage Pulsed-Power Supply," *1st IEEE Int. Conf. Sustain. Energy Technol. Syst. ICSETS 2019*, pp. 353–358, Feb. 2019, doi: 10.1109/ICSETS.2019.8745027.

[81] D. Malviya and M. Veerachary, "A Boost Converter-Based High-Voltage Pulsed-Power Supply," *IEEE Trans. Ind. Appl.*, vol. 56, no. 5, pp. 5222–5233, Sep. 2020, doi: 10.1109/TIA.2020.3007396.

[82] A. A. Elserougi, A. M. Massoud, and S. Ahmed, "A Modular High-Voltage Pulse-Generator with Sequential Charging for Water Treatment Applications," *IEEE Trans. Ind. Electron.*, vol. 63, no. 12, pp. 7898–7907, Dec. 2016, doi: 10.1109/TIE.2016.2515055.

[83] A. A. Elserougi, I. Abdelsalam, A. M. Massoud, and S. Ahmed, "A Full-Bridge Submodule-Based Modular Unipolar/Bipolar High-Voltage Pulse Generator with Sequential Charging of Capacitors," *IEEE Trans. Plasma Sci.*, vol. 45, no. 1, pp. 91–99, Jan. 2017, doi: 10.1109/TPS.2016.2633489.

[84] A. Elserougi, A. Massoud, and S. Ahmed, "Conceptual study of a Bipolar modular high voltage Pulse generator with sequential charging," *IEEE Trans. Dielectr. Electr. Insul.*, vol. 23, no. 6, pp. 3450–3457, Dec. 2016, doi: 10.1109/TDEI.2016.005803.

[85] B. W. Williams, "Power electronics : devices, drivers, applications and passive components," p. 542, 1992.

[86] I. Abdelsalam, M. A. Elgenedy, S. Ahmed, and B. W. Williams, "Full-bridge modular multilevel submodule-based high-voltage bipolar pulse generator with low-voltage DC, input for pulsed electric field applications," *IEEE Trans. Plasma Sci.*, vol. 45, no. 10, pp. 2857–2864, Oct. 2017, doi: 10.1109/TPS.2017.2743822.

[87] A. Darwish, M. A. Elgenedy, S. J. Finney, B. W. Williams, and J. R. McDonald, "A step-up modular high-voltage pulse generator based on isolated input-parallel/output-series voltage-boosting modules and modular multilevel submodules," *IEEE Trans. Ind. Electron.*, vol. 66, no. 3, pp. 2207–2216, Mar. 2019, doi: 10.1109/TIE.2017.2772189.

[88] S. Jiang et al., "A Bipolar Modular Multilevel Generator Based on Half-Bridge and Special Full-Bridge for Electroporation Applications," in IEEE Transactions on Plasma Science, vol. 49, no. 6, pp. 1920-1927, June 2021, doi: 10.1109/TPS.2021.3080327.

[89] Z. Li, X. Wang, S. Jiang, Y. Wang and J. Rao, "Research on the Bipolar Microsecond Pulse Generator Using the Multistage Resonant Charging," in IEEE Transactions on Plasma Science, vol. 50, no. 1, pp. 109-115, Jan. 2022, doi: 10.1109/TPS.2021.3133504.

[90] L. M. Redondo, M. Zahyka and A. Kandratsyeu, "Solid-State Generation of High-Frequency Burst of Bipolar Pulses for Medical Applications," in IEEE Transactions on Plasma Science, vol. 47, no. 8, pp. 4091-4095, Aug. 2019, doi: 10.1109/TPS.2019.2923570.

Mohammad Reza Qasemian Reyhan Abadi received the B.Sc. degree in electrical power engineering from Quchan University of Technology, Khorasan Razavi, Iran, in 2017. Currently, He is M.Sc. student in the field of electrical power engineering at Shahrood University of Technology, Semnan, Iran. His main research interests include modular multilevel converters, pulsed power, and renewable energy.

Mohammad Hoseintabar Marzebali received the B.Sc. degree in electrical power engineering from Mazandaran University, Mazandaran, Iran, in 2007, and the M.Sc. degree in electrical power engineering from Shiraz University of Technology, Shiraz, Iran, in 2010. In 2014, he received a scholarship from Campus France to be a joint Ph.D. as a Cotutelle Student between the University of Tehran, Tehran, Iran, and the University of Picardie ``Jules Verne," Amiens, France. Currently, he is an Assistant Professor at Shahrood University of Technology. His research interests include fault diagnose in electrical machine and modular multilevel converters.

Vahid Abolghasemi (M'12-SM'17) is currently an Assistant Professor at the School of Computer Science and Electronic Engineering, University of Essex, UK. He received the Ph.D. degree from University of Surrey, Guildford, UK in 2011. During 2011-2019, he held academic positions at Brunel University and Shahrood Univeristy of technology.
His main research interests include signal and image processing, compressive sensing, and dictionary learning. Most of his research findings and proposed solutions were published in high quality journals. He serves as a reviewer of various journals such as IEEE Transactions on Image Processing, IEEE Transactions on Signal Processing, IEEE Transactions on Neural System and Rehabilitation Engineering, etc.

Mohammad Hossein Anisi is currently an Associate Professor with the School of Computer Science and Electronic Engineering, University of Essex, U.K. and Head of Internet of Everything (IoE) Laboratory. Prior to that, he worked as a Senior Research Associate with the University of East Anglia, U.K. and Senior Lecturer with the University of Malaya, Malaysia, where he received the "Excellent Service Award" for his achievements. He has published more than 100 articles in high-quality journals and several conference papers and won two medals for his innovations from PECIPTA 2015 and IIDEX 2016 expositions. He has strong collaboration with industry and working with several companies in the UK and his research results have directly contributed to the technology industry. His research interests include IoT, WSN, Green and Energy-efficient Communication and Vehicular Networks. He has received several international and national funding awards for his fundamental and practical research as PI and Co-I. He is an Associate Editor of several journals and has been lead organizer of special sessions and workshops at IEEE conferences such as ICC, CAMAD, PIMRC, and VTC.